

Spherical harmonic modelling to ultra-high degree of Bouguer and isostatic anomalies

G. Balmino · N. Vales · S. Bonvalot · A. Briais

Received: 1 July 2011 / Accepted: 14 November 2011
© Springer-Verlag 2011

Abstract The availability of high-resolution global digital elevation data sets has raised a growing interest in the feasibility of obtaining their spherical harmonic representation at matching resolution, and from there in the modelling of induced gravity perturbations. We have therefore estimated spherical Bouguer and Airy isostatic anomalies whose spherical harmonic models are derived from the Earth's topography harmonic expansion. These spherical anomalies differ from the classical planar ones and may be used in the context of new applications. We succeeded in meeting a number of challenges to build spherical harmonic models with no theoretical limitation on the resolution. A specific algorithm was developed to enable the computation of associated Legendre functions to any degree and order. It was successfully tested up to degree 32,400. All analyses and syntheses were performed, in 64 bits arithmetic and with semi-empirical control of the significant terms to prevent from calculus underflows and overflows, according to IEEE limitations, also in preserving the speed of a specific regular grid processing scheme. Finally, the continuation from

the reference ellipsoid's surface to the Earth's surface was performed by high-order Taylor expansion with all grids of required partial derivatives being computed in parallel. The main application was the production of a $1' \times 1'$ equiangular global Bouguer anomaly grid which was computed by spherical harmonic analysis of the Earth's topography–bathymetry ETOPO1 data set up to degree and order 10,800, taking into account the precise boundaries and densities of major lakes and inner seas, with their own altitude, polar caps with bedrock information, and land areas below sea level. The harmonic coefficients for each entity were derived by analyzing the corresponding ETOPO1 part, and free surface data when required, at one arc minute resolution. The following approximations were made: the land, ocean and ice cap gravity spherical harmonic coefficients were computed up to the third degree of the altitude, and the harmonics of the other, smaller parts up to the second degree. Their sum constitutes what we call ETOPG1, the Earth's TOPography derived Gravity model at $1'$ resolution (half-wavelength). The EGM2008 gravity field model and ETOPG1 were then used to rigorously compute $1' \times 1'$ point values of surface gravity anomalies and disturbances, respectively, worldwide, at the real Earth's surface, i.e. at the lower limit of the atmosphere. The disturbance grid is the most interesting product of this study and can be used in various contexts. The surface gravity anomaly grid is an accurate product associated with EGM2008 and ETOPO1, but its gravity information contents are those of EGM2008. Our method was validated by comparison with a direct numerical integration approach applied to a test area in Morocco–South of Spain (Kuhn, private communication 2011) and the agreement was satisfactory. Finally isostatic corrections according to the Airy model, but in spherical geometry, with harmonic coefficients derived from the sets of the ETOPO1 different parts, were computed with a uniform depth of compensation of 30 km. The new

G. Balmino (✉) · N. Vales
CNES, Groupe de Recherches de Geodesie Spatiale,
Geosciences Environnement Toulouse, Observatoire
Midi-Pyrenees, 14, Avenue Edouard Belin, 31400,
Toulouse, France
e-mail: balmino@get.obs-mip.fr

S. Bonvalot
IRD, Bureau Gravimétrie International,
Geosciences Environnement Toulouse, Observatoire
Midi-Pyrenees, 14, Avenue Edouard Belin, 31400,
Toulouse, France

A. Briais
CNRS, Bureau Gravimétrie International,
Geosciences Environnement Toulouse, Observatoire Midi-Pyrenees,
14, Avenue Edouard Belin, 31400, Toulouse, France

world Bouguer and isostatic gravity maps and grids here produced will be made available through the Commission for the Geological Map of the World. Since gravity values are those of the EGM2008 model, geophysical interpretation from these products should not be done for spatial scales below 5 arc minutes (half-wavelength).

Keywords Bouguer gravity anomalies · Isostatic gravity anomalies · Earth's topography · Spherical harmonics · Surface gravity anomalies · Surface gravity perturbations

1 Introduction

The availability of high-resolution global digital elevation data sets has raised possibility to address in best conditions the basic question we want to answer: what is the Earth's gravitational potential, or gravity field when: (i) the planet is stripped of all masses above a reference surface (geoid), and (ii) mass deficiencies below the reference surface are restored to a given density.

This residual field then contains information on sub-surface density variations.

This problem has for a very long time received several solutions, especially by regional or local approximation. Considering the attraction of neighbouring topographic masses, mostly in planar geometry (local flat Earth) with some spherical correction, the computations were based on numerical integration over finite mass elements with more or less sophistication. The basics are described in several textbooks—see for instance Heiskanen and Moritz (1967), Torge (2001). This conventional approach, by which one defines classical Bouguer anomalies, is a simplified realization of the mass normalization process described above, where mass layers are usually approximated in two steps by: (i) flat plates of finite thickness, infinite extent and uniform density (Bouguer plate), (ii) volume elements, e.g. pseudo-rectangular/spherical prisms (tesseroids), to take into account the real topography of the Earth (deviation from the plates, so-called terrain correction applied at regional scale). These two steps are sometimes merged into a single one in which the total attraction of the whole mass column from the reference surface to the Earth's surface is directly computed. Moreover, the modern point of view, corresponding to Molodensky theory (see Heiskanen and Moritz 1967; and Hofmann-Wellenhof and Moritz 2005), is to stay with the attraction of the subtracted or normalized masses, at the Earth's surface; that is to compute a gravity perturbation over this surface without free-air correction. In practice, a great number of techniques and mathematical tricks have been used to improve and speed up the computational process which becomes heavy as the resolution and size of the domain increase. We will not discuss

them here since our approach is very different: it introduces a new type of anomaly and uses radically different methods.

The present study was triggered by the goal of computing a global Bouguer map, and by the work of Kuhn et al. (2009), who define and compute what they call *complete spherical Bouguer gravity anomalies* (Δg_{CSB}) using spherical terrain corrections over the whole Earth with respect to a local but full spherical Bouguer shell. Such an anomaly, at any gravity observation point P of altitude H , involves: (i) the gravitational effect of the Bouguer shell of constant thickness H and density ρ , that is $4\pi G\rho H$ (twice the value of the usual plateau term— G being the gravitational constant); and (ii) the spherical terrain correction with respect to the shell, computed over the whole planet by numerical integration over spherical volume elements having a size which increases with the distance to point P . Then the free air correction, atmospheric correction and normal gravity (at the reference ellipsoid surface) are used to achieve the computation of Δg_{CSB} . Kuhn et al. (2009) have computed high-resolution Bouguer gravity anomalies over Australia only, but it was acknowledged that the same principles can be applied globally.

Our goal has been to do a similar computation but in one step and, with some approximation, by replacing the integration stage by the use of spherical harmonic (SH) models: on the one hand models of the Earth's topography parts (lands, oceans, inner seas, lakes, polar caps) taking into account the different geometrical situations and different densities, on the other hand model of the gravity perturbations induced by the different parts or their normalized counterparts when appropriate (i.e. the replacement by material of conventional density). To do so, we used a method which we developed in a very different context, which aimed at precisely finding the gravitational spherical harmonic coefficients of a homogeneous body (an asteroid, a comet nucleus or a natural satellite of odd shape) from the spherical harmonic coefficients describing its shape (Balmino 1994). The theory also included the case of a body composed of several layers with different densities and therefore was readily applicable to the computation of the gravity perturbations due to homogeneous matter between two surfaces, which is exactly what we need here.

We define the *spherical Bouguer gravity* at the Earth's surface by:

$$g_{\text{B}}(P) = g(P) - A(\text{topo}) \quad (1)$$

where $g(P)$ is the measured gravity at point P and $A(\text{topo})$ is the total attraction (at P) of the topographic masses themselves (between the surface and the geoid) or of their substitutes according to normalization conventions. $A(\text{topo})$ is computed by taking into account the whole Earth with its real shape and surface density: topographic masses include matter above the geoid (and lack of it below the geoid in some continental areas), bathymetry, ice and lakes.

The spherical Bouguer gravity *anomaly* is then defined in the context of Molodensky theory, as:

$$\Delta g_B(P) = g_B(P) - \gamma(Q) \quad (2)$$

where $\gamma(Q)$ is the normal gravity at point Q on the telluroid, corresponding to P . Since the Molodensky (surface) anomaly is $\Delta g(\text{Molod}) = g(P) - \gamma(Q)$, we have:

$$\Delta g_B(P) = \Delta g(\text{Molod}) - A(\text{topo}) \quad (3)$$

In our case, $\Delta g(\text{Molod})$ is derived from a global Earth gravity model, here EGM2008 (Pavlis et al. 2008) and, following Pavlis (1998) and Rapp and Pavlis (1990) it is computed as:

$$\Delta g(\text{Molod}) = \left[-\frac{\partial T}{\partial r} - \frac{2}{r}T \right]_Q + \varepsilon_{\text{proj}} + \varepsilon_h + \varepsilon_\gamma \quad (4)$$

where $T = W - U$ is the disturbing gravitational potential, with W the Earth's gravity potential and U the normal potential (of the dynamic reference ellipsoid). $\varepsilon_{\text{proj}}$, ε_h , ε_γ (respectively, named isozenithal projection correction, and first and second ellipsoidal corrections) are small, long-wavelength correcting terms (not exceeding 3, 3 and 100 μGal , respectively) which we here compute from the EGM2008 spherical harmonic model truncated at degree 60. The precise evaluation on the telluroid of the term depending on T is delicate if one wants to minimize the computational effort (for very large data sets or grids)—as will be the case for the computation of $A(\text{topo})$ from spherical harmonics, and will be the subject of Sect. 4.3. Equation (3) must be slightly modified to agree with the actual definition of the reference ellipsoid which includes the mass of the atmosphere; an atmospheric correction term δg_{AC} must be *added* to the gravity anomalies. δg_{AC} is approximately a function of the elevation H with respect to sea level. With H in meters, δg_{AC} is given in milligal, by (NGA 1999):

$$\begin{aligned} \delta g_{AC} &= 0.87 \exp[-0.116(H/1,000)^{1.047}] \quad \text{if } H > 0 \\ \delta g_{AC} &= 0.87 \quad \text{if } H \leq 0 \end{aligned} \quad (5)$$

To compute $A(\text{topo})$ the core of the work has been:

- to perform spherical harmonic analysis (SHA) of the heights of the Earth's topography–bathymetry components from the ETOPO1 database (Amante and Eakins 2009) and other databases for inner seas and lakes, such as ILEC (<http://wldb.ilec.or.jp/>), at $1'$ equiangular resolution, plus SHAs of the second and third powers of these height values (as will be shown);
- then to transform the obtained SH coefficients into gravitational SH coefficients, thus producing what we call the Earth's TOPography derived Gravity model at $1'$ resolution, or ETOPG1;
- to perform spherical harmonic synthesis (SHS) of the gravity perturbations produced by ETOPG1 at the Earth's

surface $[S_E]$, defined by the lower limit of the atmosphere and based on ETOPO1 and additional data, on a worldwide $1' \times 1'$ grid;

- to perform $1' \times 1'$ SHS of the Molodensky gravity anomalies on $[S_E]$ associated with EGM2008, so as to finally produce a global spherical Bouguer gravity anomaly grid (and map).

In a similar manner, we derived the SH gravity coefficients of the compensation of all topographic components for an Airy isostatic model with fixed compensation depth, and we produced a global $1' \times 1'$ grid of the gravity corrections on $[S_E]$, and a final grid of the isostatic anomalies.

All SHAs and SHSs were done up to degree and order 10,800 corresponding to the $1'$ resolution (half-wavelength). However, for the EGM2008 surface gravity anomalies the model limitations (maximum degree and order 2,160, plus some terms up to degree and order 2,190) were obviously applied.

In a first part we will recall the theory; subsequently we will give its application to our case, emphasizing the handling of the different Earth's surface components. Then we will explain our strategy with respect to several challenging problems and describe the adopted solutions, especially concerning the SHA and synthesis of models of very high degree and order (examples will be given with verification tests and error analysis); in this part we will also address the problem of precisely and efficiently computing a geodetic function at the Earth's surface, i.e. at (a large number of) points with different altitudes, and we will give a method based on Taylor expansions of high order. These critical problems all being solved, the next part will show an example over the Morocco–South of Spain area, and comparisons with results of Kuhn (private communication 2011) using the approach of Kuhn et al. (2009) will be given. For sake of completeness, the derived Airy isostatic anomalies will also be presented over the same area (Morocco, in short). Finally we will present the worldwide $1' \times 1'$ grids and maps of spherical gravity perturbations computed from our ETOPG1 model, of spherical Bouguer anomalies derived from the EGM2008 surface gravity anomalies and from the ETOPG1 perturbations, and of Airy isostatic gravity anomalies.

2 Theory

It is based on the expression of Newton's integral in spherical harmonics, which has been addressed by many authors, e.g. Rummel et al. (1988); Balmino (1994); Wieczorek and Phillips (1998); Tsoulis (2001); Ramillien (2002); Kuhn and Featherstone (2003).

We briefly recall the basics of the method, from our earlier work (Balmino 1994). We want to find the gravitational

SH coefficients of a homogeneous body of density ρ from a SH model of its shape. In a reference coordinate system $[\mathbf{R}]$ fixed in the body, the shape is described by a truncated series S giving the radius vector r as a function of the latitude φ and longitude λ :

$$r(\varphi, \lambda) = R_0(1 + S) \quad (6)$$

where R_0 is a reference length and

$$\begin{aligned} S &= \sum_{j=0}^J \sum_{q=0}^j (\bar{A}_{jq} \cos q\lambda + \bar{B}_{jq} \sin q\lambda) \bar{P}_{jq}(\sin \varphi) \\ &= \sum_{j=0}^J \sum_{q=-j}^j \bar{T}_{jq} \bar{Y}_{jq}(\varphi, \lambda) \end{aligned} \quad (7)$$

In the case of a planetary topography, H , measured with respect to a sphere of radius R_0 , we simply have $H = R_0 S$.

In Eq. (7) the \bar{P}_{jq} are the Legendre polynomials ($q = 0$) and associated functions ($q > 0$) of the first kind, with the usual geodetic normalization (Heiskanen and Moritz 1967), the \bar{Y}_{jq} are defined by:

$$\bar{Y}_{jq}(\varphi, \lambda) = \bar{P}_{jq}(\sin \varphi) e^{iq\lambda} \quad (8)$$

$$\bar{Y}_{j,-q} = (-1)^q \bar{Y}_{jq}^* \quad (9)$$

with $q \geq 0$, $i = \sqrt{-1}$, and where the superscript * indicates the complex conjugate; coefficients \bar{A} , \bar{B} and \bar{T} are normalized according to the \bar{P} 's and \bar{Y} 's and are related by:

$$\begin{aligned} \bar{T}_{jq} &= (\bar{A}_{jq} - i\bar{B}_{jq}) / (2 - \delta_{0q}) \\ \bar{T}_{j,-q} &= (-1)^q \bar{T}_{jq}^* \end{aligned} \quad (10)$$

Let us note that we may have a \bar{T}_{00} term if $\langle r \rangle \neq 0$ (zero mean over the sphere).

On the other hand the gravitational potential of the body is also represented by a spherical harmonic series, written at each point P as:

$$\begin{aligned} U &= \frac{GM}{r} \sum_{l=0}^{l=L} \left(\frac{R}{r}\right)^l \sum_{m=0}^{+l} (\bar{C}_{lm} \cos m\lambda + \bar{S}_{lm} \sin m\lambda) \\ &\quad \times \bar{P}_{lm}(\sin \varphi) \\ &= \frac{GM}{r} \sum_{l=0}^{l=L} \left(\frac{R}{r}\right)^l \sum_{m=-l}^{+l} \bar{K}_{lm} \bar{Y}_{lm}(\varphi, \lambda) \end{aligned} \quad (11)$$

with G : the gravitational constant, M : mass of the body, R : reference length (usually close to the body mean radius), \bar{C}_{lm} , \bar{S}_{lm} and \bar{K}_{lm} : dimensionless harmonic coefficients of degree l and order m , and r , φ , λ are the spherical coordinates of the point P in the reference system $[\mathbf{R}]$. The \bar{C}_{lm} , \bar{S}_{lm} , \bar{K}_{lm} and $\bar{K}_{l,-m}$ coefficients ($m \geq 0$) are related to each other by equations similar to (10). The series for U is in principle

infinite—even if S is finite, but is truncated at degree L in practice. Here the \bar{K}_{lm} coefficients are given by:

$$\bar{K}_{lm} = \rho \alpha_{lm} \iint_{\sigma_1} \left[\int_0^{r(\varphi, \lambda)} r^{l+2} dr \right] \bar{Y}_{lm}^*(\varphi, \lambda) d\sigma_1 \quad (12)$$

where σ_1 is the unit sphere and $\alpha_{lm} = 1 / [(2 - \delta_{0m})(2l + 1) MR^l]$.

In short, we will note $\bar{T}_{jq} = (\bar{A}_{jq}, \bar{B}_{jq})^{\text{shape}}$, and $\bar{K}_{lm} = (\bar{C}_{lm}, \bar{S}_{lm})^{\text{gravit}}$. Our goal is to find the \bar{K}_{lm} 's from the \bar{T}_{jq} coefficients. The rigorous analytical solution (Balmino 1994), is quite heavy; it requires the introduction of $n - j$ coefficients (a generalization of the Clebsch–Gordan, or $3 - j$ coefficients, Wigner 1959) for the integrals of products of any number of surface spherical harmonic functions. Practical computations were performed up to degree and order 180 and for integrals of products of up to 72 functions (using a “in house” extended precision arithmetic library). We encountered numerical problems beyond those limits—which are insufficient (by far) for our concern. It is much easier to adopt the numerical solution which is recalled below.

Using Eqs. (6), (7) and (12), we find:

$$\bar{K}_{lm} = \frac{4\pi R_0^3}{(2l + 1)M} \rho \left(\frac{R_0}{R}\right)^{l+3} \sum_{k=0}^{l+3} \gamma_l^k \bar{T}_{lm}^{(k)} \quad (13)$$

with

$$\bar{T}_{lm}^{(k)} = [4\pi(2 - \delta_{0m})]^{-1} \iint_{\sigma_1} S^k(\varphi, \lambda) \bar{Y}_{lm}^*(\varphi, \lambda) d\sigma_1 \quad (14)$$

and $\gamma_l^k = \frac{1}{l+3} \binom{l+3}{k}$; $\bar{T}_{lm}^{(1)}$ is obviously equal to \bar{T}_{lm} . We note that the summation on k stops at $l + 3$ for each degree l . The $\bar{T}_{lm}^{(k)}$'s for $k > 1$ correspond to coupling (products) of the coefficients \bar{T}_{jq} (i.e. all possible combinations of k products).

The $\bar{T}_{lm}^{(k)}$ are derived by successive SHAs of the S^k function mean values computed on regular (equiangular) grids by SHS. Integrals of SH functions are computed analytically or numerically according to the degree and order (see Sect. 5.1). From this general expression we can derive formulas for different cases.

(a) Body composed of several homogeneous layers

There are $N + 1$ layers. The radius vector of the outer surface (Σ_ν) of the ν th layer ($\nu = 0, 1, \dots, N$) is modelled by:

$$r_\nu = R_\nu [1 + S_\nu(\varphi, \lambda)] \quad (15)$$

with $r_{\nu+1} < r_\nu (\forall \varphi, \lambda)$, and:

$$S_\nu(\varphi, \lambda) = \sum_{j,q} \bar{T}_{jq}^\nu \bar{Y}_{jq}(\varphi, \lambda) \quad (16)$$

As before we define:

$$\bar{T}_{lm}^{v(k)} = [4\pi(2 - \delta_{0m})]^{-1} \iint_{\sigma_1} S_v^k(\varphi, \lambda) \bar{Y}_{lm}^*(\varphi, \lambda) d\sigma \quad (17)$$

and also $\Delta\rho_v = \rho_v - \rho_{v-1}$, ($\rho_{-1} = 0$) with ρ_v the density of layer v . Introducing $\bar{\rho}$, the mean density of the body, we have:

$$\begin{aligned} \bar{K}_{lm}^{\text{gravi}}(N + 1 \text{ layers}) &= \frac{1}{\bar{\rho}} \frac{3}{2l + 1} \sum_{v=0}^N \Delta\rho_v \left(\frac{R_v}{R_0}\right)^3 \\ &\times \left(\frac{R_v}{R}\right)^l \left\{ \sum_{k=1}^{l+3} \gamma_l^k \bar{T}_{lm}^{v(k)} \right\} \end{aligned} \quad (18)$$

This equation is fundamental for deriving the Airy isostatic potential coefficients (with $N = 1$ and $R_1 = R_0 - D$, D being the depth of compensation).

(b) *Case of one layer, with density ρ_0 , limited by two complex surfaces (Σ_0) , (Σ_1)*

The radius vectors of these surfaces are defined by Eq. (15). In addition, we here assume that the layer is thin with respect to the size of the body and we take $R_1 = R_0$, which usually implies (a) nonzero \bar{T}_{00}^v term(s). Then:

$$\begin{aligned} \bar{K}_{lm}^{\text{gravi}}(\text{one layer}) &= \frac{3}{2l + 1} \frac{\rho_0}{\bar{\rho}} \left(\frac{R_0}{R}\right)^l \sum_{k=1}^{l+3} \gamma_l^k \\ &\times [\bar{T}_{lm}^{0(k)} - \bar{T}_{lm}^{1(k)}] \end{aligned} \quad (19)$$

From here we define different types of spherical harmonic coefficients representing the potential of a layer of matter, now called topography: (i) *rigorous Bouguer potential coefficients* when (Σ_1) is the Earth’s geoid, for instance defined from a global gravity field model; (ii) *ellipsoidal Bouguer potential coefficients* when (Σ_1) is an ellipsoid (of revolution); and (iii) *spherical Bouguer potential coefficients*, when (Σ_1) is a sphere of radius R_0 , given by:

$$\begin{aligned} \bar{K}_{lm}^{\text{gravi}}(\text{topo/sphere}) &= \frac{\rho_0}{\bar{\rho}} \frac{3}{2l + 1} \left(\frac{R_0}{R}\right)^l \\ &\times \left\{ \bar{T}_{lm} + \sum_{k=2}^{l+3} \gamma_l^k \bar{T}_{lm}^{(k)} \right\} \end{aligned} \quad (20)$$

The latter is the type of coefficients which will be computed and used in this paper—with the possibility of applying long wavelength ellipsoidal corrections. In the last equation, the first term ($k = 1$) has been isolated and the superscript dropped; this term is the usual single layer approximation in the transformation $\bar{T}_{jq} \rightarrow \bar{K}_{lm}$.

(c) *Case of one layer made of several parts with different densities*

An elegant way of dealing with lateral variable density is to introduce a surface density function (Kuhn and Featherstone 2003). Instead we adopted the following classical approach. We perform the above transformation (Eq. 20) for a topographic layer made of several parts of different densities corresponding to the various Earth’s surface elements and their normalization. If ρ_ω^* is the true, or normalized density, of a given component extending over a domain D_ω of the Earth, the spherical Bouguer coefficients for all components are (in shorter notation):

$$\bar{K}_{lm}(\text{topo}) = \sum_{\omega} \frac{\rho_\omega^*}{\bar{\rho}} \frac{3}{2l + 1} \left(\frac{R_0}{R}\right)^l \left\{ \bar{T}_{lm}^{\omega(1)} + \sum_{k=2}^{l+3} \gamma_l^k \bar{T}_{lm}^{\omega(k)} \right\} \quad (21)$$

The $\bar{T}_{lm}^{\omega(k)}$ harmonics are computed by SHA of topographic heights over the convex envelope of the D_ω domain solely, defined by meridians and parallels which bound the domain, and by setting the analyzed function to zero inside the envelope and outside the domain (a tapering function has been applied in some cases). Equation (21) will be truncated (as to be shown later) at $k_{\text{max}} = \min(l + 3, K)$ and will be called *transformation up to the Kth power of the topography H*, which indeed means that we take into account H/R_0 up to the power K . We pay a special attention to the degree and order zero term, given exactly by:

$$\bar{K}_{00}^{\text{gravi}}(N \text{ parts}) = \frac{3}{\bar{\rho}} \sum_{\omega=1}^N \rho_\omega^* \left[\bar{T}_{00}^{\omega(1)} + \bar{T}_{00}^{\omega(2)} + \frac{1}{3} \bar{T}_{00}^{\omega(3)} \right] \quad (22)$$

It generalises the concept of spherical Bouguer shell, and requires to carry the transformation up to $K = 3$.

Finally, and as shown in the following section, for some components of the Earth’s surface this procedure must be applied twice to account for the correct removal of some parts and normalization of others.

3 Application

We apply the above approach to the following components of the Earth’s surface (Table 1) where all elevations, taken from ETOPO1 or ILEC (or other data source in some cases) are given with respect to sea level and assumed to be orthometric heights:

- (a) all lands above or below sea-level (except the ice caps),
- (b) all oceans,
- (c) closed seas and lakes,
- (d) ice caps. Ice shelves were considered but not treated separately: assuming they are purely floating ice (ignoring the mechanical constraints at the places they are

Table 1 The different topographic components analyzed: all from ETOPO1 except closed seas and lakes (ILEC database) and ice shelves (US National Snow and Ice Data Center)

Components	Contents
Lands with $H > 0$	All—except polar caps (according to ETOPO1 data set)
Lands with $H < 0$	Chott Algeria-Tunisia, Qattara depression, Death Valley, Jordan Valley, Netherlands (part), Turfan depression
Oceans	All
Closed seas	Aral sea, Caspian sea, Dead sea
Lakes	Baikal, Balkach, Bear lake, Constance, Erie, Eyre, Huron, Ladoga, Leman, Malawi/Nyassa, Maracaibo, Michigan, Onega, Salton, Slaves (Can.), Superior, Tanganyka, Tiberiade, Titicaca, Victoria, Winnipeg, Yssyk-Koul
Ice caps	<ul style="list-style-type: none"> • Over Greenland • Over Antarctica + ice shelves (Ross, Ronne-Filchner, Larsen, Amery)

anchored on the bed-rock), their gravitational effect can be ignored.

Data errors were detected in some parts (especially the Arctic and Antarctic areas); they could be corrected under simple assumptions.

Specific polygons and grids were built to precisely delineate all different areas (e.g. lakes and seas—with their free surface altitude).

We define:

- t the elevation of the solid rock topography [called bed-rock in case (d)]; we have $t < 0$ in case (b), $t > 0$ or $t < 0$ in all other cases,
- t_0 the elevation of the closed sea or lake surface in case (c) (it may be >0 or < 0), or of the surface ice ($t_0 > 0$) in case (d),
- ρ_c the crust density, taken here equal to 2, 670 kg/m³,
- ρ_m the upper mantle density, equal to 3, 270 kg/m³,
- ρ_w the ocean density, equal to 1, 027 kg/m³,

- ρ_I the ice density, equal to 917 kg/m³,
- ρ_{sl} the density of water for inner seas and lakes; it has been assigned a constant value for a given entity although some are known to have parts with different densities,
- $\rho^* = \rho_{sl}$ in case (c), $\rho^* = \rho_I$ in case (d):

Figure 1 illustrates cases (c) and (d)—other cases are well known.

3.1 Digital terrain model (DTM)-induced gravity disturbance (DIG)

This is the gravity field induced by the topographic-water-ice masses and their normalization, computed from a given DTM, here ETOPO1.

The computation of such a field to produce Bouguer anomalies implies in each case the following “removal” of surface densities (in the algebraic sense—it is indeed an addition in some configurations):

- (a) $t \rho_c$
- (b) $t (\rho_c - \rho_w)$
- (c), (d) $(t_0 - t)\rho^*$ and $t\rho_c$.

Equation (21) is applied in each case. Note that this is the correct sign for these quantities when computing the $\bar{K}_{lm}(\text{topo})$, i.e. the coefficients of the DTM-induced gravity disturbance field itself.

3.2 Airy isostatic compensation

In this well-known model the topographic constructs float on the upper mantle, a denser under-layer of constant density ρ_m ; therefore we have roots or anti-roots under the topographic components.

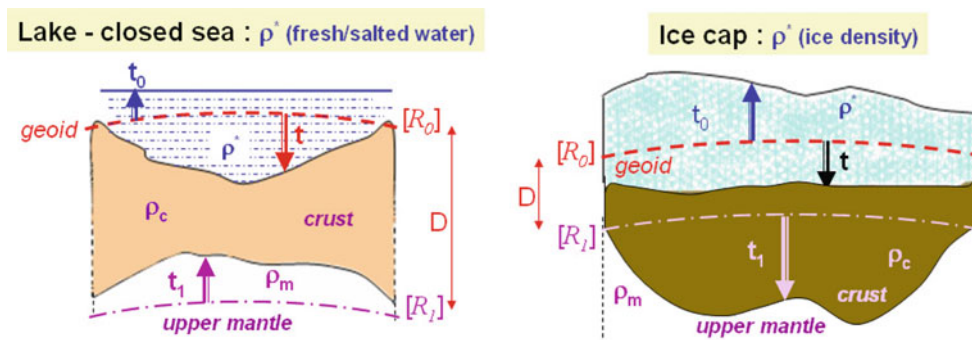


Fig. 1 Geometry of considered layers for closed seas and lakes and for ice caps, and of Airy isostatic model for these cases. t_1 is the elevation of the root (or anti-root) at compensation level (of depth D)

Let us further define:

- $\Delta\rho_0 = \rho_c$ in case (a), $\Delta\rho_0 = \rho_c - \rho_w$ in case (b)
- $\Delta\rho_1 = \rho_m - \rho_c$
- $\Delta\rho^* = \rho_c - \rho^*$ where, as before, $\rho^* = \rho_{sl}$ in case (c), $\rho^* = \rho_I$ in case (d)—cf. Fig. 1.

Then, adopting a depth of compensation D , that is a level at which the pressure induced by all surface loads is constant, we can compute the elevation t_1 of the roots or anti-roots, measured with respect to the sphere of radius $R_1 = R_0 - D$:

- cases (a) and (b):
$$t_1 = -t \frac{\Delta\rho_0}{\Delta\rho_1} \left(\frac{R_0}{R_1}\right)^2 \tag{23}$$

- cases (c) and (d):
$$t_1 = -\left[t \frac{\Delta\rho^*}{\Delta\rho_1} + t_0 \frac{\rho^*}{\Delta\rho_1} \right] \left(\frac{R_0}{R_1}\right)^2 \tag{24}$$

The factor $(R_0/R_1)^2$ accounts for the ratio of the surface elements sustained by the same solid angle, at levels R_0 and R_1 , which enter into the equilibrium equation; it is equal to one in planar geometry. Equation (23) was already derived by Rummel et al. (1988). Using Eq. (18) with solely the $\nu = 1$ term (to isolate the compensation part), we find the corrections to the gravitational SH coefficients due to t_1 :

- for cases (a) and (b), a formula in which the $\bar{T}_{lm}^{(k)}$ enter directly, thus not requiring any additional SHA:

$$\begin{aligned} \Delta\bar{K}_{lm}(\text{Airy}) &= \sum_{\text{lands}}^{\text{oceans}} \left[\frac{3}{2l+1} \frac{\Delta\rho_0}{\bar{\rho}} \left(\frac{R_0}{R}\right)^l \right. \\ &\quad \times \sum_{k=1}^{l+3} \gamma_l^k (-1)^k \left(\frac{\Delta\rho_0}{\Delta\rho_1}\right)^{k-1} \\ &\quad \left. \times \left(\frac{R_0 - D}{R_0}\right)^{l+3-3k} \bar{T}_{lm}^{(k)} \right] \tag{25} \end{aligned}$$

- for case (c) or (d):

$$\begin{aligned} \Delta\bar{K}_{lm}(\text{Airy}) &= -\frac{3}{2l+1} \frac{\Delta\rho_1}{\bar{\rho}} \left(\frac{R_0 - D}{R_0}\right)^3 \left(\frac{R_0 - D}{R}\right)^l \\ &\quad \times \sum_{k=1}^{l+3} \gamma_l^k \bar{T}_{lm}^{1(k)} \tag{26} \end{aligned}$$

with $\bar{T}_{lm}^{1(k)}$ being the SH coefficients of t_1 as given by (24) and obtained by SHA.

In all cases, with the signs adopted in the last two equations, the $\Delta\bar{K}_{lm}$ coefficients must be *added* to the Bouguer *anomaly* field coefficients to obtain the isostatic anomalies.

4 Challenging problems and strategies

As we have seen it, the theory is fairly simple and adopting the numerical approach makes the problem tractable, provided that we meet some challenges related to the desired resolution of the representation, which we want to match the information contents in the ETOPO1 database.

4.1 The meaning of spherical DIG potential coefficients

We made several approximations from which geometrical origin is shown in Fig. 2.

Rigorously one should analyze OS/ R_0 and OG/ R_0 (Fig. 2a) and their successive powers to get the SH coefficients $\bar{T}_{lm}^{0(k)}$ and $\bar{T}_{lm}^{1(k)}$ according to formula (19). Firstly we ignore the geoid height, because: (i) its maximum value ($\sim \pm 100$ m) is much smaller than H in most places on Earth; (ii) the computation of the terrain effect is then made independent of the geoid model; (iii) it makes the computational effort smaller; (iv) comparisons with other approaches in spherical geometry are easier; (v) the impact of any geoid model may be evaluated subsequently. Secondly, H being given as a function of the geodetic latitude Φ (and longitude λ), we map H onto the sphere with the geocentric latitude φ (properly converted from Φ) instead of φ' (Fig. 2b). This is justified by the fact that (Fig. 2c): $\varphi' - \varphi \approx f \sin 2\Phi H/R_0$ is always $< 2.10^{-4}$ degree (0.8'') in absolute value, and also: $|H' - H| \approx |H|(\Phi - \varphi)^2/2 < 0.06$ m. The analyses of all functions $(H/R_0)^k$ being done in such spherical approximation, the synthesis (computation of grids) will be performed in accordance. However, it may be interesting to quantify it with respect to the ellipsoidal approximation. Assuming $H' = H$ and $\varphi' = \varphi$ (Fig. 2d), the correction (to be *added* to the spherical DIG potential coefficients) is, following Eq. (12):

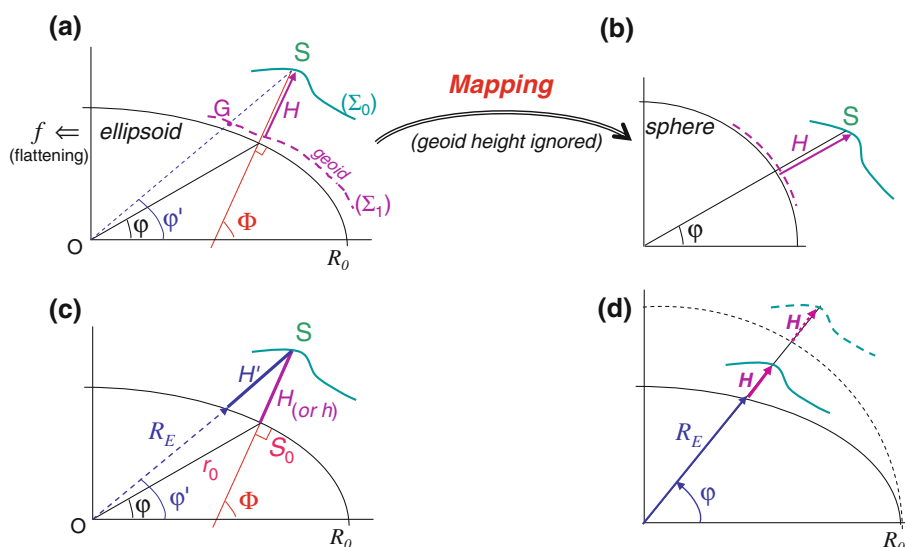
$$\begin{aligned} \delta\bar{K}_{lm} &= \rho\alpha_{lm} \iint_{\sigma_1} \left[\int_{R_E(\varphi)}^{R_E(\varphi)+H} r^{l+2} dr - \int_{R_0}^{R_0+H} r^{l+2} dr \right] \\ &\quad \times \bar{Y}_{lm}^*(\varphi, \lambda) d\sigma_1 \tag{27} \end{aligned}$$

The difference of the two integrals is:

$$\Delta_l = \sum_{k=1}^{l+3} \gamma_l^k [R_E^{l+3-k} - R_0^{l+3-k}] H^k \tag{28}$$

where one may take $R_E(\varphi) = R_0(1 - \varepsilon_2 \sin^2 \varphi + \varepsilon_4 \sin^4 \varphi - \dots)$ with sufficient accuracy and $\varepsilon_2, \varepsilon_4$ being given in terms

Fig. 2 Approximations made in the analysis of the topography and the derivation of spherical DIG potential coefficients. **a** Given $H(\varphi, \lambda)$, GS should be analyzed (for rigorous DIG coefficients); **b** H is mapped on the sphere; **c** the difference $H - H'$ can be neglected (h is introduced in the context of Sect. 4.3); **d** origin of the ellipsoidal correction



of the reference ellipsoid second eccentricity e' , or its flattening f ($\varepsilon_2 = \frac{1}{2}e'^2 \approx f$; $\varepsilon_4 = \frac{3}{8}e'^4 \approx \frac{3}{2}f^2$).

H is written $H = R_0 \sum_{j,q} \bar{T}_{jq} \bar{Y}_{jq}(\varphi, \lambda)$ and corrections are then obtained by transforming the products $\sin^2 \varphi \bar{Y}_{jq}(\varphi, \lambda)$ and $\sin^4 \varphi \bar{Y}_{jq}(\varphi, \lambda)$, and using the orthogonality property of the $\bar{Y}_{jq}(\varphi, \lambda)$ functions (Balmino 2003). We only give here corrections of first order in f and first and second order in H/R_0 ; we write $\delta \bar{K}_{lm} = \delta^1 \bar{K}_{lm} + \delta^2 \bar{K}_{lm}$ with:

$$\delta^k \bar{K}_{lm} = -(l + 3 - k)\varepsilon_2 [a_{l-2,m} \bar{T}_{l-2,m}^{(k)} + b_{lm} \bar{T}_{l,m}^{(k)} + c_{l+2,m} \bar{T}_{l+2,m}^{(k)}] \quad (29)$$

The a, b, c coefficients are given by:

$$\begin{aligned} a_{nk} &= \frac{1}{2n + 3} \\ &\times \left[\frac{(n - k + 1)(n - k + 2)}{2n + 1} \frac{(n + k + 1)(n + k + 2)}{2n + 5} \right]^{1/2} \\ c_{nk} &= \frac{1}{2n - 1} \left[\frac{(n - k)(n - k - 1)}{2n - 3} \frac{(n + k)(n + k - 1)}{2n + 1} \right]^{1/2} \\ b_{nk} &= \frac{2n(n + 1) - 2k^2 - 1}{(2n - 1)(2n + 3)} \end{aligned} \quad (30)$$

(they are =0 whenever $n < 0$ or $k > n$).

Of greater interest are the long wavelength corrections which we have computed in parallel to the correcting terms considered for the surface gravity anomalies (see Sect. 1). They will be shown later on together with other results.

4.2 Spherical harmonic functions of high degree and order

There has been an increasing need in resolution and precision of SH representations in the last years, which has generally

followed our increase of knowledge of the Earth's topography or other geophysical or geographical functions. SH functions need to be computed up to degree and order (d/o) 10,800 in the present work, which corresponds to the 1' resolution (half-wavelength) of ETOPO1, and soon to d/o 21,600 if one wants to represent the data sets which become available at the 30'' resolution (~1 km). The problem which plagues most algorithms is of numerical nature and is due to the Institute of Electrical and Electronic Engineers' (IEEE) standard for binary floating-point arithmetic; this limits the range of all real numbers which can be represented on current computers to $\sim 10^{-305}$ to $\sim 10^{+305}$. In particular, the computation of all SH functions for high d/o cannot be done without several tricks, which may be costly.

There is no problem with the Legendre polynomials, only with the associated Legendre functions (ALF): $\bar{P}_{lm}(x)$, $x = \sin \varphi$, $m > 0$. Writing these as $y^m \bar{H}_{lm}(x)$, where $y = \cos \varphi$ and $\bar{H}_{lm}(x)$ = polynomial of degree $l - m$, the problem is known to come from both terms and is exemplified in Fig. 3a for $l = 21,600$ and on Fig. 3b for $m = 3,600$ (computations have been done with a special in-house library developed by the first author for demanding celestial mechanics applications).

Figure 3a shows that $\bar{P}_{lm}(x)$ becomes nonsignificant above some maximum order, a phenomenon used by Jekeli et al. (2007)—see below. On Fig. 3b it is clear that the \bar{H}_{lm} 's increase regularly with l before becoming significant, then oscillate around a stable value; and the \bar{P}_{lm} 's behave similarly (starting at $\sim \cos m\varphi$), which we will use in our algorithm.

When using recursive relations on the $\bar{H}_{lm}(x)$, as it has become customary in geodesy, usual tricks, e.g. Wenzel single normalization (1998), or Horner's schemes (in $\cos \varphi$) on partial sums such as in Holmes and Featherstone (2002),

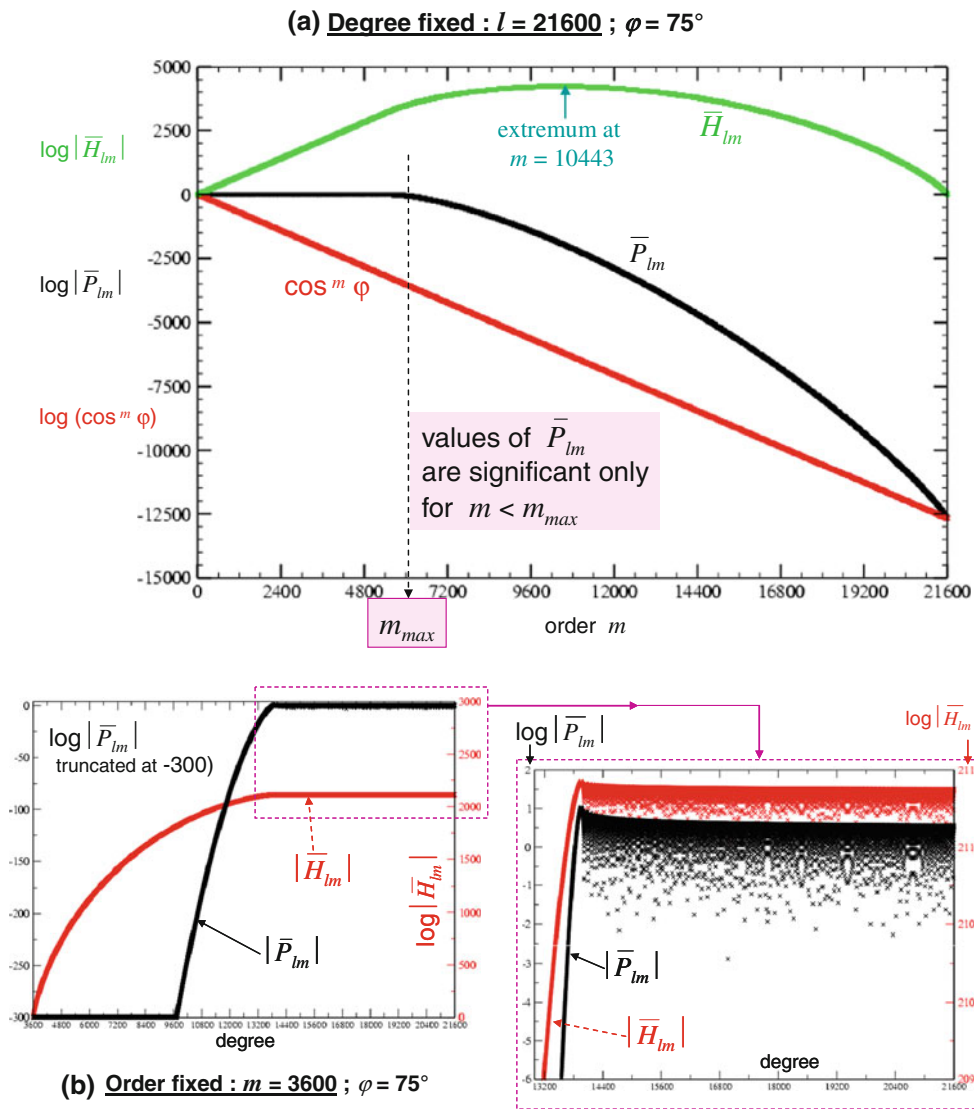


Fig. 3 Behaviour of the Legendre associated functions $\bar{P}_{lm}(x)$, and their components $\cos^m \varphi$ and $\bar{H}_{lm}(x)$, at 75° North latitude: **a** for degree 21,600 and all orders; **b** for order 3,600 ($\cos^m \varphi = 10^{-2.113}$) and degrees up to 21,600

do not work at such level. Use of specialized library is an alternative but is too time consuming for operational situations. A breakthrough was made recently (Jekeli et al. 2007) which started from the recognised fact that the *meaningful* ALFs at a given latitude and for a given degree follow a semi-empirical rule which allows to safely neglect more and more terms—indeed to limit the order of the expansion, as $|\varphi|$ increases (cf. Fig. 3a), to $m_{\max}(\varphi, l) = l \cos \varphi + C$ (C is an empirical constant depending on the spectrum of the studied function); this circumvents all numerical problems provided that one makes use of recursive formulas for the $\bar{P}_{lm}(x)$ themselves with fixed degree (which are in principle unstable near the poles). Based on Fig. 3b, our approach has been to modify Jekeli et al.’s strategy by working *by order*—

therefore by converting their limiting criterion: for a given latitude φ and fixed order m , we retain the terms of degree $l > l_0(m) - D(m, \varphi)$, where $l_0(m)$ is derived from Jekeli et al.’s rule (except near the poles where we adopted a different formulation) and D is an empirical function (Fig. 4). By computing the $\bar{H}_{lm}(x)$ by recursive formulas with fixed order (stable close to poles) we take advantage of the Partial Sums-Longitude Recursion (PSLR) technique for the SHS of equiangular grids (Bosch 1983) and its dual formulation (LRPS) in SHA (Balmino 2003)—all this in view of the existing software developed along many years. Besides we can retain 64 bits arithmetic, though making verifications in 128 bits, for optimization purposes (on small computers), without losing precision near the poles. The drawback is that

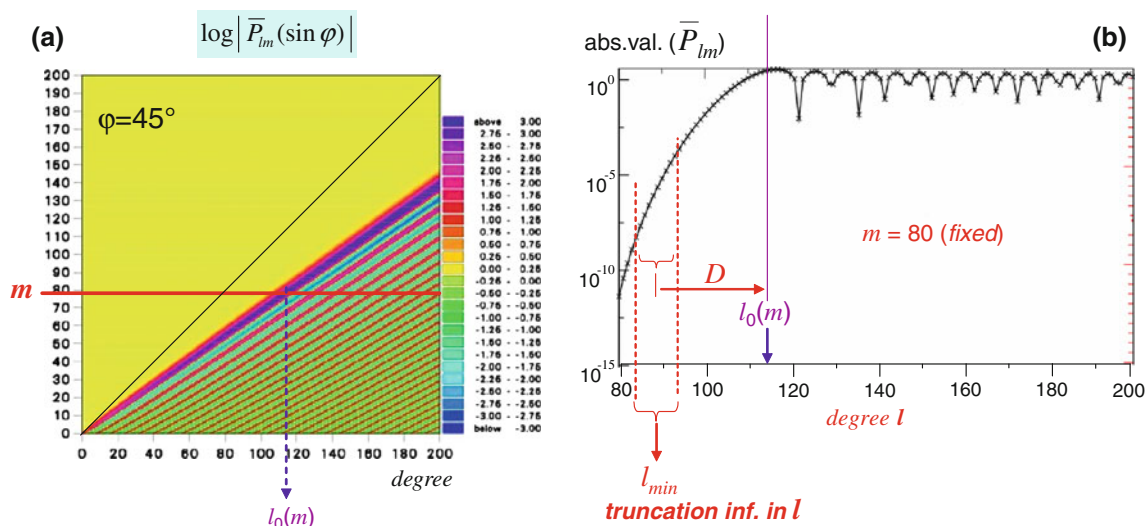


Fig. 4 Example of Jekeli et al.'s (2007) criterion transposed to the case of associated Legendre functions of fixed order and variable degree. φ being fixed, $\overline{P}_{lm}(\sin \varphi)$ increases regularly with l , up to $l \sim l_0(m)$, then

oscillates around a stable value. The significant degrees are retained above $l_{\min}(m) = l_0(m) - D(m, \varphi)$ where D is an empirical function

we have to compute some intermediate values of the $\overline{H}_{lm}(x)$ which are out of the IEEE range but necessary for starting the scheme. The core of the algorithm is described in appendix A and is based on the idea of Wenzel (1998); it consists in an iterated re-normalization of the $\overline{H}_{lm}(x)$ as l increases. Finally, depending on the maximum degree and latitude, we apply Horner's schemes in $\cos \varphi$ and (or) with respect to the normalization factor.

4.3 Precise and efficient computation of a geodetic function at the Earth's surface

The Bouguer correction, or the isostatic one, is a gravity perturbation $\delta g = -\partial T / \partial r$ and must be computed at the Earth's surface $[S_E]$, that is at variable altitude for each point. This hampers the application of fast techniques (such as PSLR) in SHS. The problem is general and we must question ourselves on the accuracy of usual methods for gridding values of any geodetic function on $[S_E]$ from a high d/o SH model, such as the surface gravity anomalies—for instance derived from a global model like EGM2008.

Most of the time, the function is gridded on the *ellipsoid*, then upward (or downward) continued (using 1st, 2nd, ... derivatives—also evaluated on the same grid). This is hardly sufficient in high mountains, even for expansions up to 2,160 (2190) like in EGM2008 as we are going to see it. First, all altitudes (H) of ETOPO1 and altitudes of the lakes and closed seas are converted to ellipsoidal altitudes (h) using EGM2008. The surface of the oceans is assumed to coincide with the geoid. Therefore, $[S_E]$ is referred to the EGM2008 ellipsoid. For surface (Molodensky) gravity anomalies Δg

the computation is done on the telluroid and we assimilate the ETOPO1 elevations to normal altitudes, equal to zero over the oceans.

The rigorous calculation of $\delta g(S)$ or $\Delta g(S)$ is too heavy, since it requires to recompute the ALFs at each point S (see Fig. 2c), but it has been done over limited mountainous areas for verification. We may adopt a semi-rigorous method: we already noted that the latitude difference $\varphi - \varphi'$ remains quite small even for significant altitudes (for instance it is 0.0001208° at 4,000 m and latitude $\varphi = 45^\circ$). Therefore the ALFs need not be recomputed at each grid point but solely once for each parallel (but the exact radius vector value at each point S is used). We have inter-compared these methods for computing Δg , also with the upward continuation from the ellipsoid using Taylor expansions of order 1 and order 2, over a $2^\circ \times 2^\circ$ part of the Atlas mountains in Morocco where H ranges from 134 to 3,785 m, and using EGM2008. Results are given in Table 2.

Obviously the rigorous method is very costly. The semi-rigorous method works very well in terms of precision and can be taken as reference. The Taylor expansions are not precise enough at this level. Looking at the first (radial) and second derivatives of Δg (Δg_1 and Δg_2), it appears that these terms, evaluated with EGM2008, are unrealistically large over the highest mountain summits ($< 5\%$ of the area): Δg_1 reaches -0.492 and 0.376 mGal/m (this is greater than the free-air gradient!) and Δg_2 ranges from -5.0610^{-4} to $+5.4910^{-4}$ mGal/m²; elsewhere Δg_1 is ~ 0.01 mGal/m and $\Delta g_2 \sim O(10^{-5})$ mGal/m². Consequently we experimented more with the semi-rigorous method but found that it was costly at high resolution ($1' \times 1'$

Table 2 Comparison of different SHS methods: $5' \times 5'$ grids of surface gravity anomalies (in mGal) over part of the Atlas mountains, from EGM2008 and elevation data set DTM2006

Method	Min. value	Max. value	r.m.s. differences (mGal)	CPU time ^a
(1) Rigorous	-41.39	249.12	-	761
(2) Semi-rigorous	-41.39	249.05	(2)-(1): 0.004	73
(3) Taylor 1	-41.30	237.02	(3)-(2): 4.783	10
(4) Taylor 2	-41.39	255.30	(4)-(2): 2.070	16

^a IBM Power 5 (1.9 GHz) processor—time in seconds

Table 3 Computation of $1' \times 1'$ grids of δg at degree and order 10,800 by the semi-rigorous method; comparison of CPU time over areas of different sizes (IBM Power 5 (1.9 GHz) processor)

Area	Latitude extension	Longitude extension	CPU time (sec)
Everest	1°	2°	7,363
France	9.5°	13.5°	247,301
Morocco	11°	12°	316,902

grids with d/o 10,800) over large areas (see Table 3—with some anticipation on the Bouguer gravity field model, ETOPG1, which we obtained from ETOPO1 and other data, and which will be described in Sect. 5). Although computations over the whole Earth could be done with it, we decided to re-visit the Taylor expansion approach to save computer time.

Any degree l component of a geodetic functional has the factor $(a/r)^l$ where a is a reference length (close to the Earth’s equatorial radius). We want to study the convergence of the following Taylor expansion of order N around r_0 and for various values of r (see Fig. 2c, with $r = OS$ and $r_0 = OS_0$):

$$\left(\frac{a}{r}\right)^l = \left(\frac{a}{r_0}\right)^l + \sum_{k=1}^N \frac{1}{k!} \left[\frac{\partial^k (a/r)^l}{\partial r^k} \right]_{r=r_0} (r - r_0)^k \quad (31)$$

We test the convergence in spherical approximation; we expand $(a/r)^l$ with $r_0 = a$, $r = a + h$, around $h = 0$, that is:

$$\left(\frac{a}{r}\right)^l = 1 + \sum_{k=1}^N \frac{(-1)^k}{k!} \Pi_l^k \left(\frac{h}{a}\right)^k \quad (32)$$

where $\Pi_l^k = \prod_{j=0}^{k-1} (l + j)$.

Results, as shown on Fig. 5, are striking: one needs to go to very high orders N as the elevation increases, all the more as the degree increases too.

Those findings are for individual terms, and may be tempered by considering the (decreasing) values of the function SH coefficients. Also one has to weigh the performances of the method with respect to the semi-rigorous approach.

Indeed we have been able to implement the simultaneous computation of a geodetic function and its radial derivatives of high order, and the final summation at grid nodes, in a quite efficient way. Details are given in Appendix B. Then we have been able to compare the two approaches. Anticipating once more on the obtained ETOPG1 model (see next section) we have computed grids of gravity perturbations δg on $[S_E]$ over several areas and for varying orders N of the Taylor expansion (Table 4).

The conclusions are:

- CPU time t is clearly linear in N : for example in the case of Everest $t \approx 1,750 + 11.5N$; but it does not increase much with N (cf. France area);
- the computer time saving with respect to the semi-rigorous method is more than an order of magnitude over large areas;
- $N = 40$ will ensure a precision always better than ~ 0.1 mGal (worst case over Everest) and certainly much better (few microgals) almost everywhere on Earth.

Therefore Taylor expansion with $N = 40$ has been adopted for all subsequent SHS of grids.

5 Main results

5.1 Analysis of the Earth’s topography

The SH coefficients $\overline{T}_{lm}^{(k)}$ are derived by a standard quadrature method applied to $1' \times 1'$ equiangular mean values, and accelerated by the Longitude Recursion-Partial Sums algorithm (LRPS, Balmino 1994). Integrals of ALFs are computed in different ways according to the order m and the maximum degree L : the method of Gerstl (1980) is applied up to d/o 1,800 or above for low orders, then a modification of it (Balmino 2003) is used up to d/o 2,700 or above for low m (with one initial normalization); beyond those limits, numerical Simpson method is applied (with subdivision of the integration interval when necessary) on the ALFs computed according to Appendix A. De-smoothing

Fig. 5 Investigation on the Taylor expansion order required to compute $(a/r)^l$ at the Earth's surface by upward continuation from the ellipsoid. **a** Degree $l = 2,160$; **b** degree $l = 10,800$

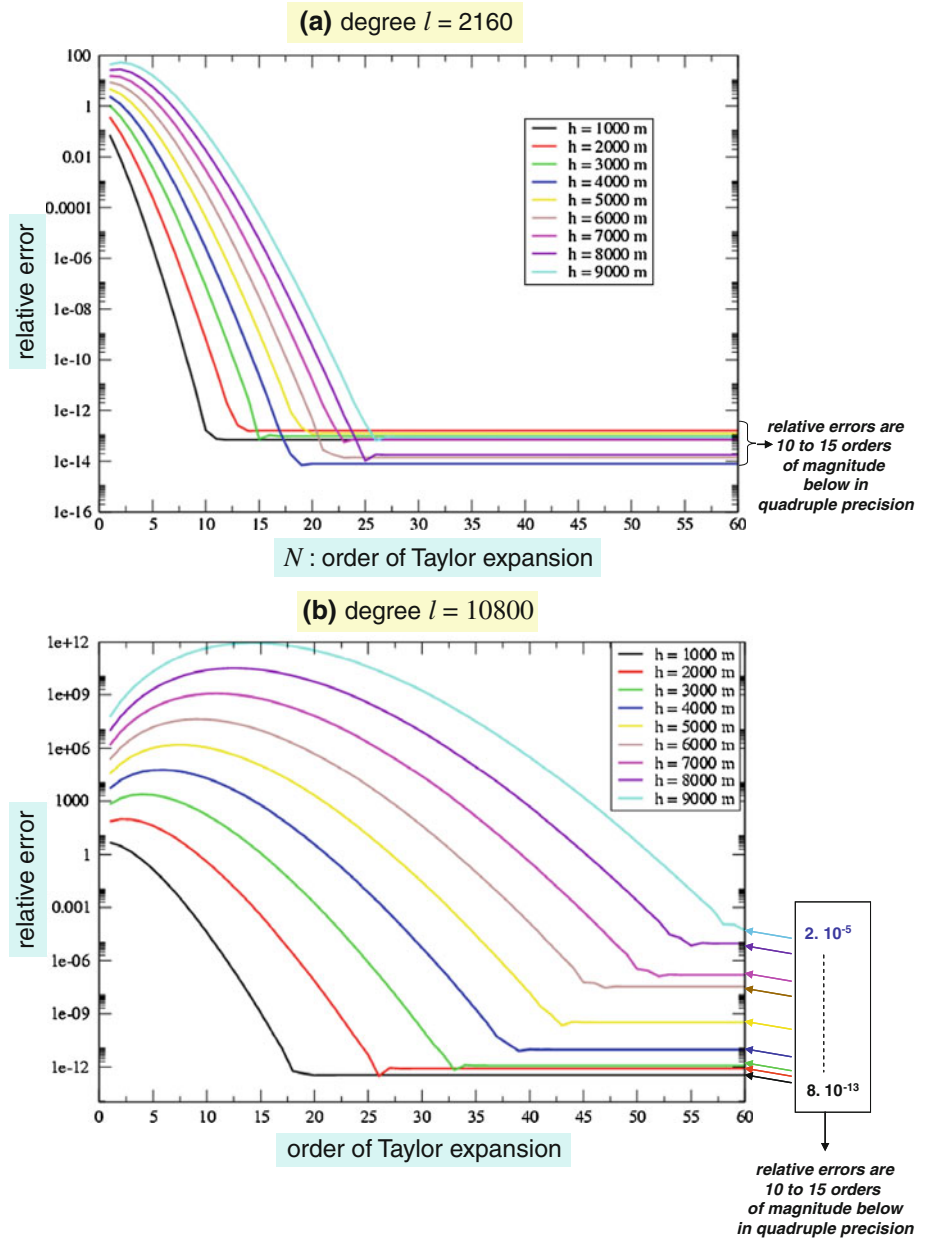


Table 4 Computation of gravity perturbations δg with full ETOPG1 model ($l_{max} = 10,800$) at ETOPO1 points ($1' \times 1'$ grids): (i) by Taylor expansion; (ii) by semi-rigorous method

Area ↓	lat. min/max long. min/max	N (Taylor)	min/max diff. with semi-rig. method (mGal)	CPU time (sec)	CPU time semi-rig. method (sec)
Everest	27.5°/ 28.5° 86.0°/ 88.0°	30	- 4.27 / + 39.51	2094	7363
		35	- 1.20 / + 23.74	2145	
		40	- 0.13 / + 0.004	2205	
		60	- 4.10 ⁻⁷ / + 1.10 ⁻⁷	2438	
France	42.0°/ 51.5° - 5.0°/ 8.5°	20	- 1.16 / + 0.06	14525	247301
		30	- 3.10 ⁻⁵ / + 3.10 ⁻⁵	15696	
Morocco	28.0°/ 39.0° - 12.0°/ 0.0°	30	- 5.10 ⁻⁷ / + 5.10 ⁻⁷	20391	316902

Comparison of performances for various orders N

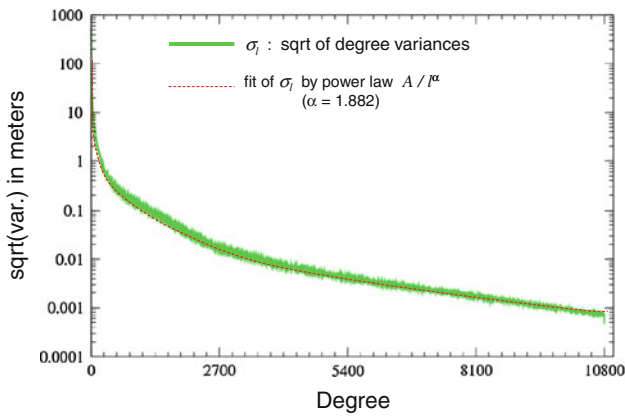
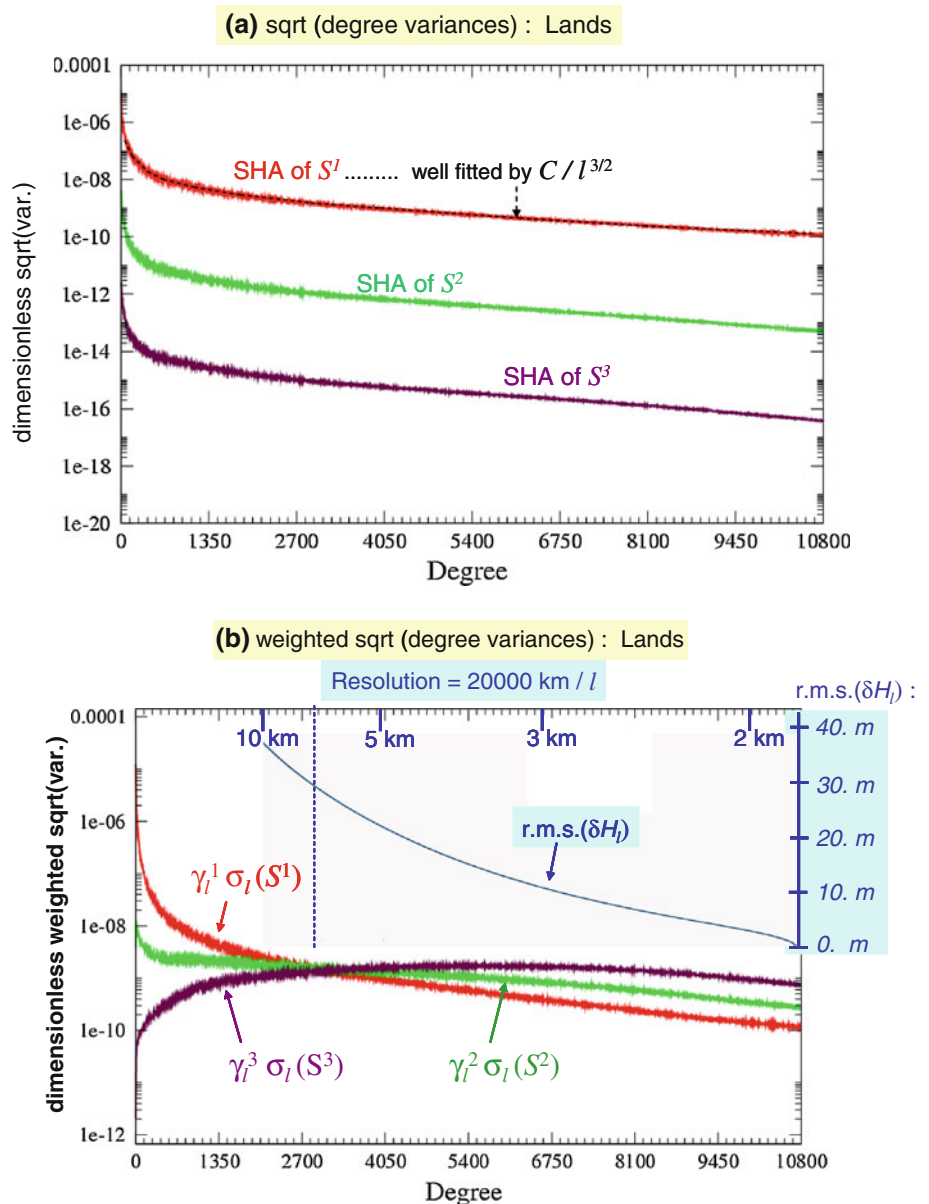


Fig. 6 Results of analysis of the whole Earth topography (land topo. and oceans/lakes bathymetry) from ETOPO1: square root of SH coefficients degree variances (in meter)

Fig. 7 Spectral behaviour of the SH coefficients $\overline{T}_{lm}^{(k)}$ for the lands only (excluding lakes, closed seas and ice covered parts) up to $k = 3$. **a** S^k stands for the k th power of the land topography; **b** The coefficients $\overline{T}_{lm}^{(k)}$ are weighted by γ_l^k , and shown with respect to the contribution to topography, r.m.s. (δH_l), of harmonics of degree $> l$



factors based on Meissl–Pellinen coefficients (Jekeli 1981) are finally introduced.

Figure 6 shows the behaviour of the SH coefficients (here multiplied by R_0) resulting from the analysis of ETOPO1 data set. An empirical law: $A/l^{1.882}$ fits well with these spectral components.

We then look at the magnitude of the SH harmonics of the k th power of the topography. Figure 7 shows their dimensionless spectral components; at first glance one would decide that going beyond $k = 3$ is superfluous (Fig. 7a), but the gravitational contribution of the $\overline{T}_{lm}^{(k)}$ must be weighted by γ_l^k (Fig. 7b): higher-order terms ($k > 1$) become much more important at resolution higher than ~ 7 km ($l > 2,800 = l_0$); this contradicts a statement of Wieczorek and Phillips (1998) on the decrease of these terms. This might be also

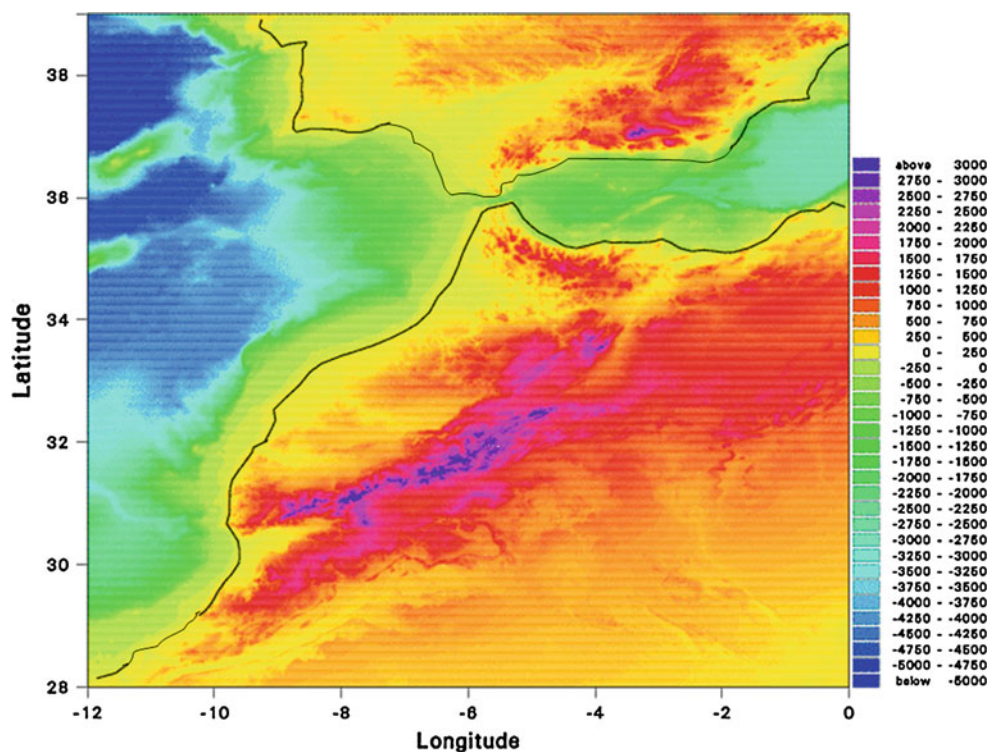


Fig. 8 Morocco–South of Spain–ocean area, selected for many tests and comparisons in this study. Topography is from ETOPO1; values are between $-5,247$ and $3,771$ m

true for $k > 3$ (which we have not investigated). However, Fig. 7b also shows that the contribution to topography, r.m.s. $(\delta H_l) = R_0 * \text{r.m.s.}[\bar{T}_{lm}^{(1)}]$, of those terms of degree $> l_0$ is rather small. This is why we decided to truncate expansion (13) at $k = 3$ at most; this is in agreement with Wiczorek (2007). Nevertheless this remains, at this stage, an empirical approximation which demands external comparison (see Sect. 6).

Next we investigated the precision of our SHA of the topography, by recomputing (by SHS to d/o 10,800) $1' \times 1'$ mean values and comparing them with the original ETOPO1 mean values, to quantify the error on the DTM-induced gravity field—which we do in Sect. 5.2. We did it for many areas on Earth; the largest differences appear over the Himalayas (25°N to 40°N , 70°W to 95°W) with: $\text{min} = -196$ m, $\text{max} = +167$ m, $\text{r.m.s.} = 12.8$ m. We then selected an area which we found quite representative of the Earth's relief in terms of topographic features and values: Morocco–South of Spain (Morocco area in short). It has mountainous and flat parts, significant bathymetry and its topography ranges from $-5,247$ to $+3,771$ m (Fig. 8). It will be used subsequently for testing several steps of our approach.

The evaluation of the precision of our SHA–SHS procedures over this area (Fig. 9) shows acceptable differences, although geographically correlated: differences are larger over highest and rough topography (Fig. 9a) as could be

intuitively expected; this is confirmed by a close look at a West–East 200-km long section which crosses rough topography and then a more gentle area (right of Fig. 9b) where smaller differences are visible. We call this *error of representation*, which may be attributed to both the SHA and the SHS which are approximations of exact operators—SHS is not exactly the inverse of SHA.

We can further perform a SHA of this error, then a new SH of the differences and see if the process converges. Results over the test area are given in Table 5. There is indeed a sign of convergence, but is it worth the effort? We will answer it in the next section.

5.2 The ETOPO1-induced gravity disturbance model

This model results from the conversion into gravitational SH coefficients, of the sets of SH coefficients representing the Earth's topography (lands, oceans, ice caps and underlying bed-rock) provided by the ETOPO1 database, plus elevation data of main closed seas and large lakes, as explained in the previous sections. It may be symbolically noted $\{\bar{K}_{lm}(\bar{T}_{jq})\}$. It is complete to d/o 10,800. The behaviour of its spectral components is shown on Fig. 10. Compared to the EGM2008 characteristics (to d/o 2,160), it is obvious that they are significantly larger, the well known sign of a compensation mechanism such as isostasy.

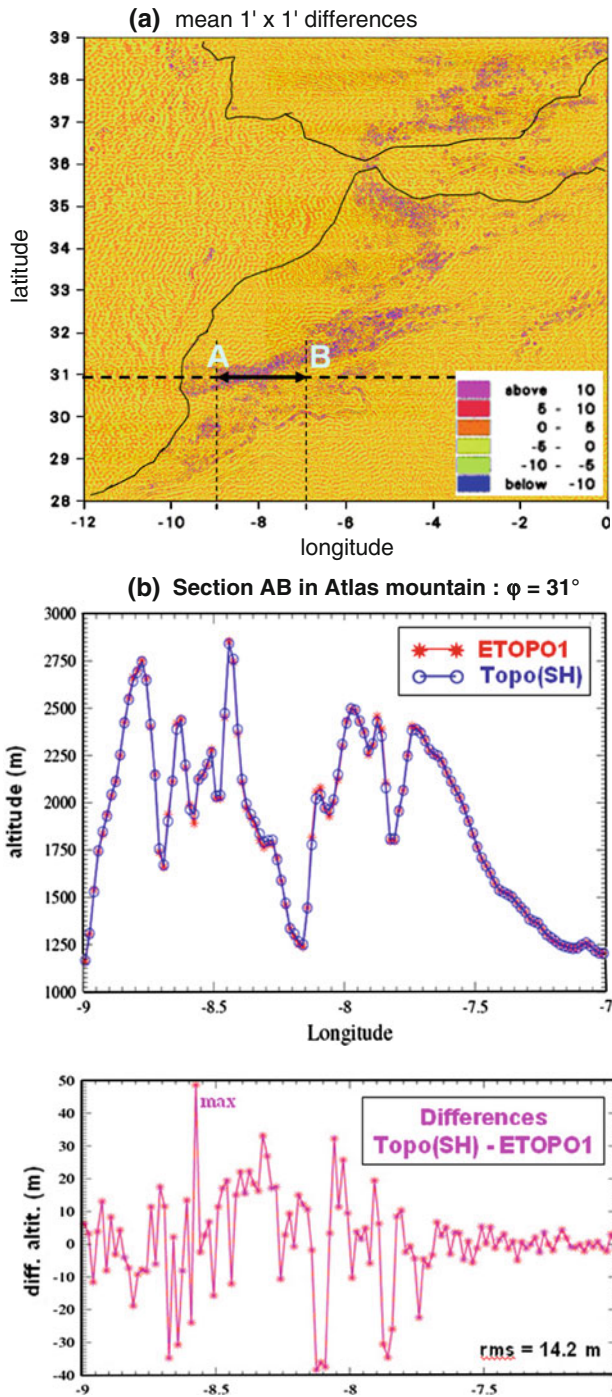


Fig. 9 Error of representation of the topography in the test area: differences between the recomputed topography (from SH) and ETOPO1. **a** Over the whole area: *min/max/r.m.s.* = -67, +67, 4.2 m; **b** comparison along section AB: the fit is much better when altitude gradients are small (here East of longitude -7.7°)

The model has uncertainties coming from the errors in the original data sets. Some, of tens or even hundreds of meters, were discovered in the ETOPO1 data, e.g. over the Dead Sea and Jordan Valley, over lake Titicaca, . . . (we could correct for some of them). In addition, there is an error coming

Table 5 Reduction of the error of representation of the topography (in meter) by iterated SHA–SHS

Iter.→	0	1	2
Min	-66.8	-44.6	-40.4
Max	+67.3	+44.0	+41.6
r.m.s.	4.2	2.7	2.5

Morocco test area

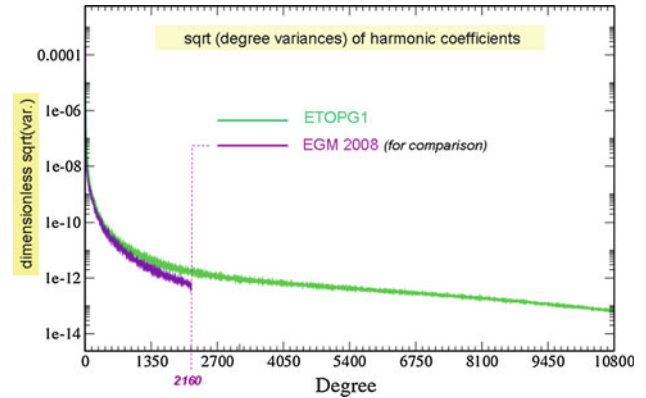


Fig. 10 Spectral characteristics of the ETOPG1 field model to degree 10,800, compared to EGM2008 to degree 2,160

from the error of representation of the topography by SH (see Sect. 5.1). The impact of the former is difficult to clarify. To try to quantify the latter we may evaluate the global r.m.s. error on the induced gravity perturbation δg . We start from:

$$\delta g(r, \varphi, \lambda) = \frac{GM}{a^2} \sum_l (l + 1) \left(\frac{a}{r}\right)^{l+2} \sum_m \bar{K}_{lm} \bar{Y}_{lm}(\varphi, \lambda) \tag{33}$$

We propagate the variances and we average over the unit sphere σ_1 :

$$\langle \sigma^2(\delta g) \rangle_{\sigma_1} \approx \left(\frac{GM}{a^2}\right)^2 \sum_l (l + 1)^2 \sum_m \langle \sigma^2(\bar{K}_{lm}) \rangle \tag{34}$$

We make a single layer approximation with the surface density ρ equal everywhere to ρ_c (equivalent rock topography), that is:

$$\bar{K}_{lm} \approx \frac{\rho}{\bar{\rho}} \frac{3}{2l + 1} \bar{T}_{lm} \tag{35}$$

Using:

$$\sum_l \sum_m \langle \sigma^2(\bar{T}_{lm}) \rangle \approx \frac{\langle \sigma^2(\delta H) \rangle}{R_0^2} \tag{36}$$

where $\langle \sigma^2(\delta H) \rangle^{1/2}$ is approximated by *r.m.s.*(δH), the mean error of representation, we find:

$$r.m.s.(\delta g) = \{ \langle \sigma^2(\delta g) \rangle_{\sigma_1} \}^{1/2} \approx \frac{3}{2} \frac{GM}{a^2} \frac{\rho}{\bar{\rho}} \frac{r.m.s.(\delta H)}{R_0} \tag{37}$$

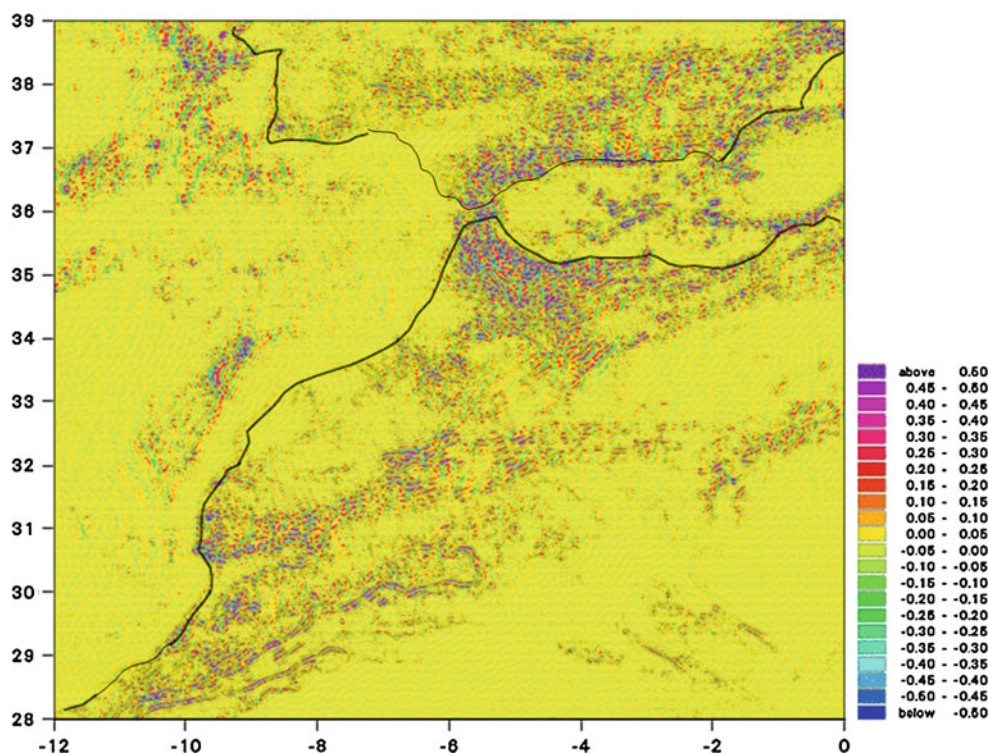


Fig. 11 Error on DTM-induced gravity disturbance δg due to estimated error of representation of the topography by SH, over the Morocco test area. min = -2.2 mGal; max = $+2.2$ mGal; r.m.s. = 0.12 mGal

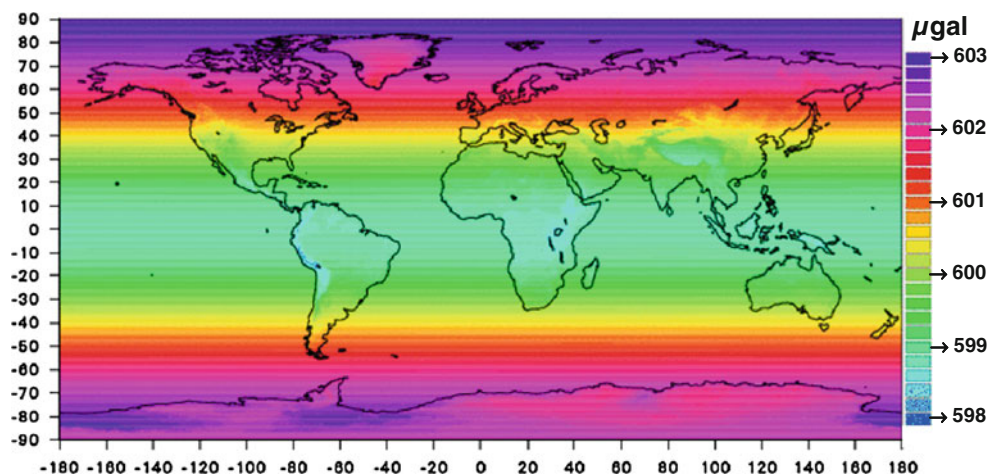


Fig. 12 Ellipsoidal correction on the gravity perturbations, limited to degree and order 120. It ranges between 598 and 603 μGal

If we take $r.m.s.(\delta H) \approx 4$ m (cf. Morocco area—representative of Earth), we have $r.m.s.(\delta g) \approx 0.5$ mGal for the whole Earth, which is rather small compared to other error sources (errors in ETOPO1 as said above, in the reference global gravity field model used to compute surface anomalies...). This is confirmed by a direct computation over the Morocco test area, Fig. 11) where the full error of representation (at iteration 0—see Table 5) is analyzed and converted into errors

on gravitational harmonics. Therefore, we decided not to perform several SHA–SHS iterations worldwide.

Finally we computed the ellipsoidal corrections on the gravity perturbations (Fig. 12), to d/o 60, then to d/o 120—which did not make significant difference. They exhibit long wavelength patterns with prominent zonal components and have a magnitude around 0.5 mGal. They may be applied or not depending on the usage of ETOPO1.

5.3 The derived Airy isostatic model

We computed the SH coefficient corrections according to Sect. 3.2 with a constant compensation depth $D = 30$ km.

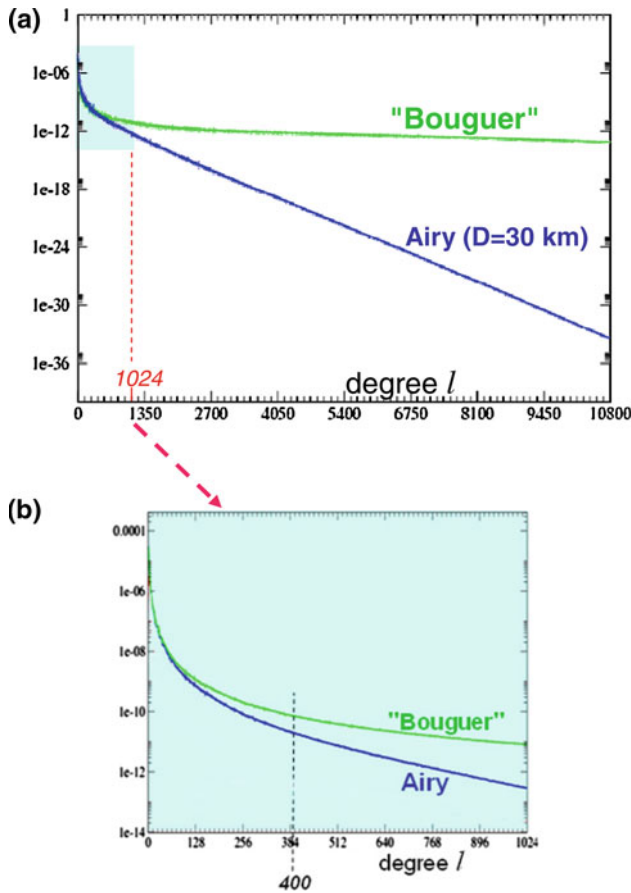


Fig. 13 Comparison of the spectral components of the ETOPO1-induced gravity disturbance and Airy isostatic field (fixed compensation depth $D = 30$ km)

Obviously the mean magnitude of the $\Delta \bar{K}_{lm}$ coefficients decreases very quickly due to the factor $[(R_0 - D)/R_0]^l$, which is confirmed on Fig. 13: around degree 400, Airy correction is smaller than the topographic effect by a factor of ~ 5 , and it is more than an order of magnitude below it at degree $\sim 1,000$; then it becomes negligible for larger degrees. We call δg_{ISO} the gravity perturbations derived from $\Delta \bar{K}_{lm}$, to be added to the Bouguer anomalies so as to obtain the usual isostatic anomalies (Sect. 3.2).

At regional scale, we compare the DTM-induced gravity disturbances and the isostatic corrections over our test area. The former have been limited to degree 400 for sake of magnitude comparison and for enhancing geographical correlation. As can be seen from Fig. 14, the Airy model removes a significant part to the topographic masses' gravitational effect.

6 External comparison

As discussed in Sect. 5.1 a critical point in our approach is the truncation (at $k = 3$) of the expansion giving the gravitational SH coefficients in terms of the harmonics of the relative elevations H/R_0 at the k th power. Outside validation only can bring confidence (or not) on this choice. The most reliable way of doing it is the direct numerical integration of the attraction of the topographic masses effect (and/or of their normalization), which has been the approach of Kuhn et al. (2009). As recalled in Sect. 1, Kuhn uses a numerical scheme where the gravity contribution at point P of the whole topography is computed over the full sphere by quadrature over the topographic masses elements having a size which increases with the distance to point P (to reduce the computational effort).

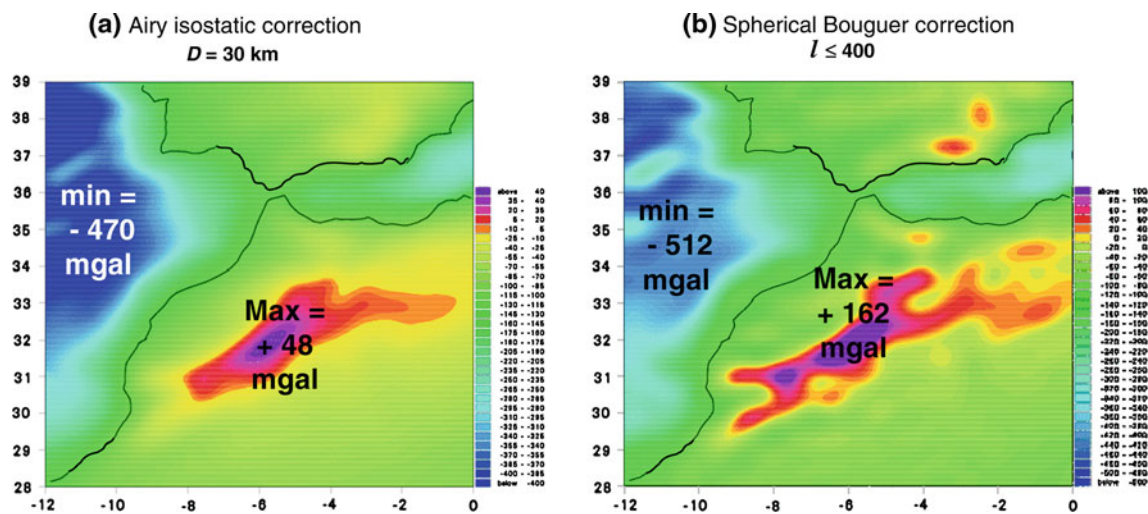


Fig. 14 Airy isostatic corrections over the Morocco test area, with a compensation depth of 30 km (a); and DTM-induced gravity disturbances (here labelled spherical Bouguer corrections) to degree 400 (b)

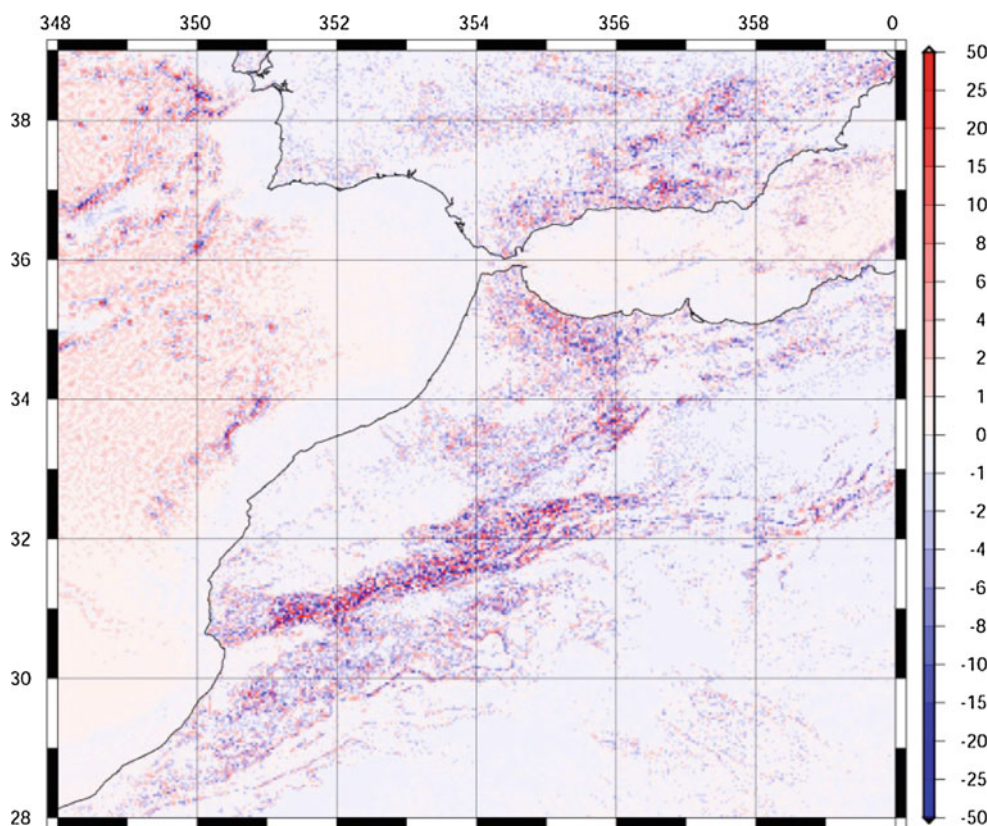


Fig. 15 Difference between the combined DTM (ETOPO1)-induced gravitational effect from Newtonian integration based on point values (grid/node registered data) and the spherical harmonic approach (this

paper) over the Morocco–South of Spain test area; min = -37.344 , max = 48.040 , mean = -0.067 , SD = 2.340 (Unit: mGal). (Kuhn, private communication 2011)

Kuhn (private communication 2011) nicely provided a test computation over the Morocco area. He made two calculations: one based on ETOPO1 mean (cell/pixel) values and another one based on ETOPO1 point (grid/node) values. In the latter case, the values are taken as mean values of a block shifted by half a grid element. In both instances, the computational point (i.e. at which the gravity disturbance is evaluated) is the center of each considered block. Therefore Kuhn's second case was retained for comparison, which is summarized by the difference map in Fig. 15.

There is almost no bias (-0.067 mGal) in the differences which is not surprising since our truncation limit ($k = 3$) ensures that the \overline{K}_{00} term is computed with no approximation. The agreement is fairly good on average with a standard deviation of 2.34 mGal. However, the minimum and maximum values and the geographical distribution of the differences (which exhibit a clear correlation with the topography) probably indicate that the truncation at the third power of the elevation is not sufficient in areas of high/rough topography at such high resolution. Finally part of the difference may also be attributed to the effective spatial resolution of the spherical harmonic models at d/o 10,800 and to Gibbs effect of which the SHAs suffer when modelling step functions.

7 Worldwide maps of spherical Bouguer anomalies and isostatic corrections

The different parts of the global, spherical approach which we explained in the preceding sections, have been applied to the production of several $1' \times 1'$ grids (and maps) in the context of the “World Gravity Map” project of the Commission for the Geological Map of the World (CGMW 2010). The project, sponsored by UNESCO, consists in the production of a new worldwide Bouguer anomaly map. We therefore computed four main grids, all of them on the physical Earth's surface (lower limit of the atmosphere); they are point values at the nodes of the ETOPO1 equiangular mesh.

- Surface gravity anomalies (Δg) from EGM2008: this computation was of course done up to the maximum degree (2,159, plus terms up to 2,190) of the reference model (Fig. 16).
- Gravity perturbations (δg) from the ETOPG1 model, to d/o 10,800 (Fig. 17).
- Spherical Bouguer anomalies (Δg_B): by subtracting the grid (δg) from the (Δg) one (Fig. 18).
- Isostatic corrections (δg_{ISO}) according to the Airy model with a 30 km compensation depth: the computation was

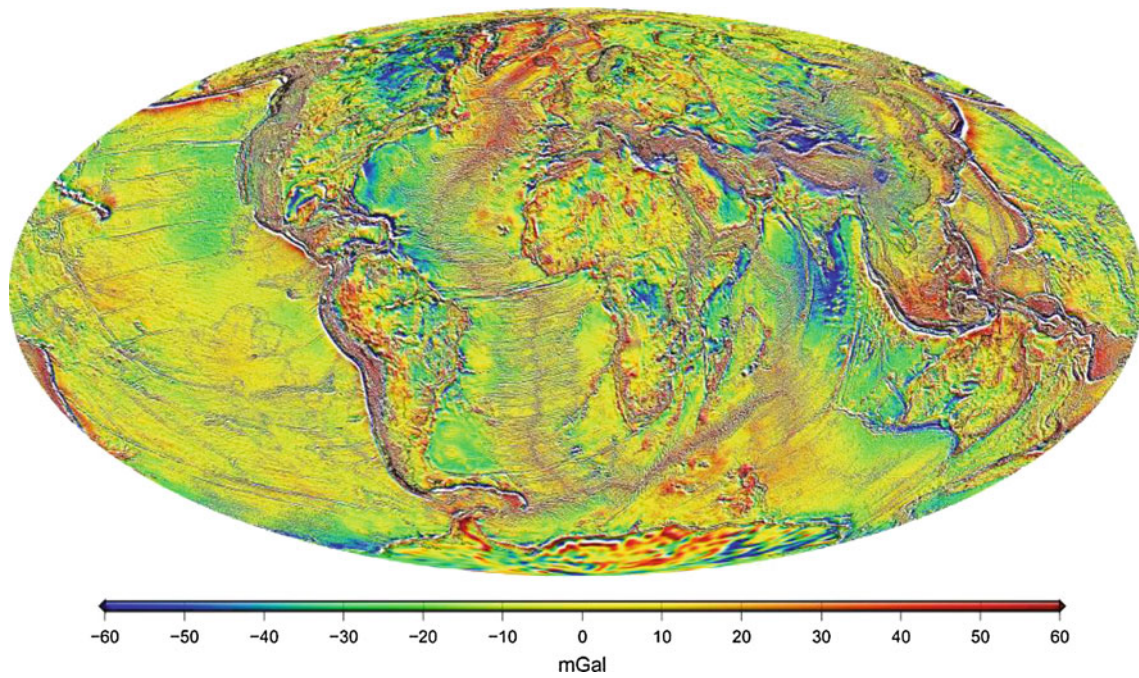


Fig. 16 Surface (Molodensky) gravity anomalies from EGM2008 and ETOPO1; min = -364 mGal, max = $+670$ mGal

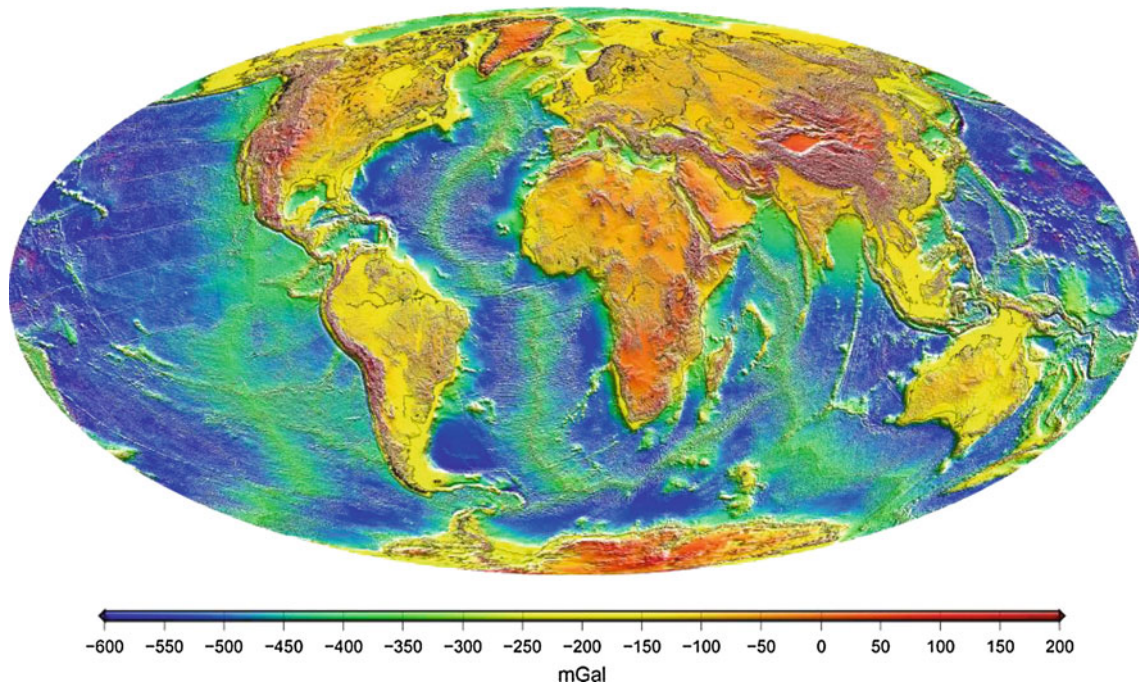


Fig. 17 Gravity perturbations (ETOPG1) from ETOPO1, at Earth's surface; min = $-1,123$ mGal, max = $+626$ mGal

done only to d/o 2,160—which is by far sufficient considering the spectral decay of the Airy isostatic correction SH coefficients (Fig. 19).

Other grids have been derived such as the one of isostatic anomalies (by adding Δg_B and δg_{ISO}). They will be analyzed and documented by the CGMW project committee.

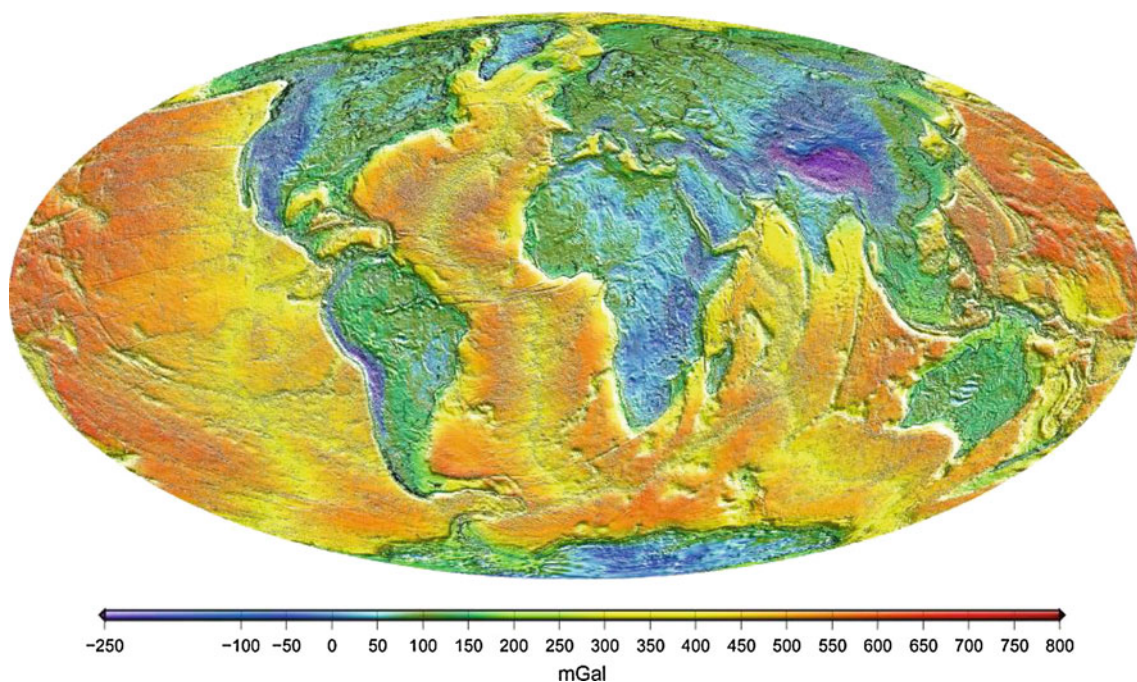


Fig. 18 World spherical Bouguer anomalies from EGM2008 and ETOPO1; min = -529 mGal, max = $+1,005$ mGal

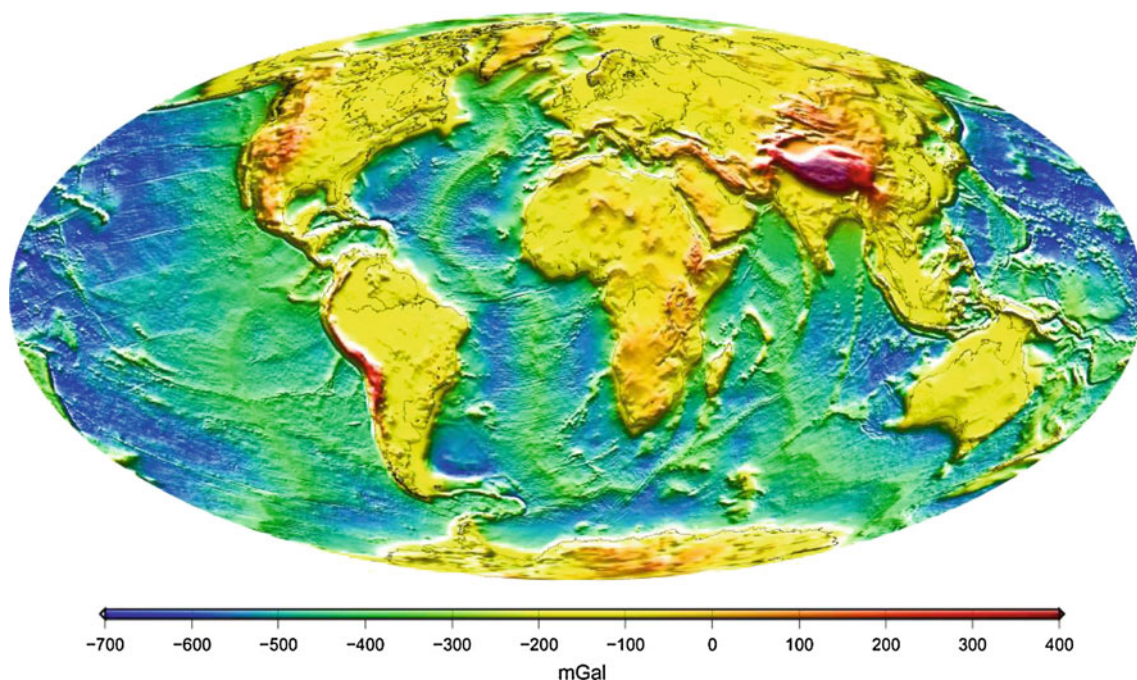


Fig. 19 Airy isostatic corrections derived from ETOPO1; depth of compensation is 30 km; min = -761 mGal, max = $+460$ mGal

8 Conclusions

We have designed a way to handle global topography and derived gravity at a very high resolution through SHA and synthesis, though with some approximation. The present work has established and used expansions up to degree and order 10,800, compatible with the $1'$ resolution of

the available data set. Thanks to the approach, especially the successive re-normalization strategy in the computation of spherical harmonic functions, we do not foresee limitations in the mid-future when higher resolution data sets are used. The method has been validated in one case but this test is incomplete; further verification will be necessary.

The way Bouguer, and also isostatic anomalies, are understood and computed differs from the common usage, but meets modern concerns which tend to take the real Earth into account.

A $1' \times 1'$ grid of worldwide surface gravity perturbations has been computed from the ETOPO1 data set and other data for lakes and closed seas, taking into account usual normalization conventions for the densities of various topographic components. Higher-resolution terrain corrections may benefit from it by integrating residual topography up to shorter distances. $1' \times 1'$ grids of spherical Bouguer anomalies and of spherical Airy isostatic corrections have also been produced.

The philosophy behind this novel computation of a so-called “complete spherical Bouguer anomaly” will be clarified with respect to different communities of users in the context of the World Gravity Anomaly Maps to be published by CGMW.

Acknowledgments This research was supported by the CNES Programme Directorate and the Toulouse Space Center, the Centre National de la Recherche Scientifique and the Institut National des Sciences de l’Univers, the Institut de Recherche pour le Développement. We especially thank Michael Kuhn who kindly applied his method over the Morocco area for comparison with our method. We thank the reviewers who made very detailed and constructive comments.

Appendix A: computation of associated Legendre functions (ALF) of very high degree

We compute the $\bar{H}_{lm}(x)$ by standard stable recursion with fixed order m , variable degree l from m to L . The recursion is modified by a normalization factor which is applied several times, as becomes necessary with respect to the IEEE limitations on real numbers.

We make choice of a factor f , very small but larger (by 10 to 20 orders of magnitude) than the smallest real number which the computer can represent. For instance $f = 10^{-280}$. We then define $G=1/f$. We initialize a counter $N_f = 0$ and a table $\nu(k)$ by $\nu(0) = m - 1$; then we compute:

$$\begin{aligned} \tilde{H}_{0,0} &= f; \tilde{H}_{1,1} = \sqrt{3} f; \tilde{H}_{l,l} = \sqrt{1 + 1/(2l)} \\ \tilde{H}_{l-1,l-1} &\text{ for } l \geq 2 \\ \tilde{H}_{l,l-1} &= x \sqrt{2l + 1} \tilde{H}_{l-1,l-1}; \quad l \geq 1 \\ \tilde{H}_{lm}^{(x)} &= \alpha_l^m [x \tilde{H}_{l-1,m}(x) - \tilde{H}_{l-2,m}(x)/\alpha_{l-1}^m]; \\ l \geq 2, \quad 0 \leq m \leq l - 2 \dots \quad (R) \end{aligned}$$

where $\alpha_l^m = [(2l - 1)(2l + 1)/[(l - m)(l + m)]]^{1/2}$

We apply (R), with m fixed and l variable (from m to L), as long as $|\tilde{H}_{lm}(x)| < G$.

As soon as this condition is not verified, and if $m < L$:

- we increment N_f by 1
- we define : $\nu(N_f) = l$

- we multiply $\tilde{H}_{lm}(x)$ and $\tilde{H}_{l-1,m}(x)$ by f
- we continue the recursion in l .

The process is iterated (still with m fixed), each time we have $|\tilde{H}_{lm}(x)| \geq G$. At the end $\tilde{H}_{\nu(k),m}$ and $\tilde{H}_{\nu(k)-1,m}$ are divided by f , for $k = 1, \dots, N_f$, and we define $\nu(N_f + 1) = L$.

We note that $N_f = 0$ if the condition $|\tilde{H}_{lm}(x)| \geq G$ was never fulfilled. For a given value $\tilde{H}_{lm}(x)$ (m fixed) there is a k for which $\nu(k) < l \leq \nu(k + 1)$; therefore its true value is:

$$\bar{H}_{lm}(x) = \tilde{H}_{lm}(x)/f^{k+1}$$

It cannot be written as such in most cases if it exceeds the IEEE range $[10^{-s}, 10^{+s}]$ but instead we get its logarithmic value:

$$\log |\bar{H}_{lm}(x)| = -(k + 1) \log f + \log |\tilde{H}_{lm}(x)|$$

with $\text{sign}[\bar{H}_{lm}(x)] = \text{sign}[\tilde{H}_{lm}(x)]$.

Finally the value of the ALF is obtained as follows:

$$\text{Let } Z = \log |\bar{P}_{lm}(x)| = m \log(\cos\varphi) - (k + 1) \log f + \log |\tilde{H}_{lm}(x)|$$

- if $Z < -s$: $\bar{P}_{lm}(x) = 0$. (it is actually an *underflow*)
- if not: $\bar{P}_{lm}(x) = 10^Z \times \text{sign} [\tilde{H}_{lm}(x)]$

In practice, we never encountered an *overflow*. As an example, in the case of Fig. 3b the algorithm finds six normalizations: $\nu(1) = 4,418$, $\nu(2) = 5,098$, $\nu(3) = 5,988$, $\nu(4) = 7,156$, $\nu(5) = 8,735$ and $\nu(6) = 11,110$.

Actually we have seen that we can take into account the ALFs for $l > l_{\min} = l_0(m) - D(m, \varphi)$ only, that is we do not have to recover the ALFs, as shown above, for $l \leq l_{\min}$ which is some time saving. The determination of l_{\min} is semi-empirical. It has been established by numerous tests up to $d/0.32,400$.

L being the maximum degree we define $K = 20 + 8.10^{-3}L$ and $d_L = \frac{3}{2}\pi/L$ (this is $1.5 \times$ the maximum resolution). For a given latitude φ , that is at polar distance $d = 90 - |\varphi|$:

- the overall computation is carried up to:

$$\begin{aligned} m_{\max}(L) &= \min[L \cos\varphi + K, L] \\ \text{or } \max [35 - 5 \log_2(d_L/d), 0] &\text{ if } d < d_L \text{ and } L > 720 \\ \{\text{d-condition}\} \end{aligned}$$

- for each order $m \leq l \leq L$, from $m_{\max}(L)$ to 1 because computations are done in reverse order (in m and in l) for improved accuracy:

$$\begin{aligned} m \leq l \cos\varphi + K &\Rightarrow l_{\min} = \max[m, (m - K)/\cos\varphi] \\ \text{or } m \leq 35 - 5 \log_2(d_l/d) &\Rightarrow l_{\min} = \frac{3\pi}{2} \frac{1}{d^{27-m/5}} \text{ if} \\ \{\text{d-condition}\} &\text{ is true.} \end{aligned}$$

Appendix B: implementation of the Taylor expansion method

Let us consider a geodetic functional written as: $F(r, \varphi, \lambda) = w(r, \varphi) f(r, \varphi, \lambda)$ with:

$$f(r, \varphi, \lambda) = \frac{GM}{a^q} \sum_{m=0}^L \left[\sum_{l=m}^L \left(\frac{a}{r} \right)^{l+q} \delta_l (\bar{C}_{lm} \cos m\lambda + \bar{S}_{lm} \sin m\lambda) \bar{P}_{lm}(\sin \varphi) \right]$$

and where $w(r, \varphi)$, q and δ_l are given by the table below for the quasi-geoid height (ζ), the gravity anomaly Δg and the gravity perturbation (or disturbance) δg .

Param.	$w(r, \varphi)$	q	δ_l
F			
ζ	$1/\gamma(r^*, \varphi)$	1	1.
Δg	1	2	$l-1$
δg	1	2	$l+1$

In the case of ζ , r^* is at the telluroid and is (in principle) obtained by iteration. The Taylor expansion of order N is:

$$f(r, \varphi, \lambda) = \sum_{k=0}^N \Delta^k \left(\frac{r-r_0}{a} \right)^k$$

with $\Delta^k = \frac{GM}{a^q} \frac{(-1)^k}{k!} \sum_{m=0}^L \Delta_m^k$

We now use the PSLR technique (Bosch 1983); each Δ_m^k is written as:

$$\Delta_m^k = A_m^k \cos m\lambda + B_m^k \sin m\lambda$$

and (PS part of the algorithm):

$$\begin{bmatrix} A_m^k \\ B_m^k \end{bmatrix} = \sum_{l=m}^L \left(\frac{a}{r_0} \right)^{l+q+k} \delta_l \Pi_{l+q}^k \bar{P}_{lm}(\sin \varphi) \begin{bmatrix} \bar{C}_{lm} \\ \bar{S}_{lm} \end{bmatrix}$$

where the Π_{l+q}^k have been defined in the text.

(φ, λ) being now a grid node (φ_i, λ_j) with $\lambda_j = \lambda_0 + j\Delta\lambda$, (λ_0 : origin of longitudes, $\Delta\lambda$: grid stepsize in longitude), all $\Delta_m^k(\lambda_j) = \Delta_{m,j}^k$ are computed simultaneously by (LR part of the scheme):

$$\Delta_{m,j}^k = 2 \cos m\Delta\lambda \Delta_{m,j-1}^k - \Delta_{m,j-2}^k$$

This recursion is initialized by $\Delta_{m,0}^k = \Delta_m^k(\lambda_0)$ and $\Delta_{m,1}^k = \Delta_m^k(\lambda_1)$.

References

Amante C, Eakins BW (2009) ETOPO1 1 arc-minute global relief model: procedures, data sources and analysis. NOAA Technical Memorandum NESDIS NGDC-24, Boulder (Co)

- Balmino G (1994) Gravitational potential harmonics from the shape of an homogeneous body. *Cel Mech Dyn Astr* 60(3):331–364
- Balmino G (2003) Ellipsoidal corrections to spherical harmonics of surface phenomena gravitational effects. *Festschrift zum 70. Geburtstag von H. Moritz*, Publication of Graz Techn. University, pp 21–30
- Bosch W (1983) Effiziente Algorithmen zur Berechnung von Raster-Punkwerten von Kugelfunktionsentwicklungen. Memorandum, D.G.F.I., Munich
- Commission for the Geological Map of the World-CGMW (2010) Resolutions of the CGMW General Assembly, UNESCO, Paris
- Gerstl M (1980) On the recursive computation of the integrals of the associated Legendre functions. *Manuscr Geod* 5:181–199
- Heiskanen WA, Moritz H (1967) *Physical Geodesy*. Freeman and co, San Francisco
- Hofmann-Wellenhof B, Moritz H (2005) *Physical Geodesy*. Springer, Berlin
- Holmes SA, Featherstone WE (2002) A unified approach to the Clenshaw summation and the recursive computation of very high degree and order normalised associated Legendre functions. *J Geod* 76:279–299
- Jekeli C (1981) Alternative methods to smooth the Earth's gravity field, Rep N0.310, Department of Geodetic Science and Surveying, Ohio State University, Columbus
- Jekeli C, Lee KJ, Kwon JH (2007) On the computation and approximation of ultra-high-degree spherical harmonic series. *J Geod* 81:603–615
- Kuhn M, Featherstone WE (2003) On the optimal spatial resolution of crustal mass distributions for forward gravity field modelling. In: *Gravity and geoid 2002*, Proceedings, pp 195–200
- Kuhn M, Featherstone WE, Kirby JF (2009) Complete spherical Bouguer gravity anomalies over Australia. *Aust J Earth Sci* 56:213–223
- NGA (1999) Gravity station data format and anomaly computations. Technical Report, Geospatial Sciences Division, St Louis (Mo)
- Pavlis NK (1988) Modeling and estimation of a low degree geopotential model from terrestrial gravity data. Rep. N0. 386, Dpt. of Geodetic Sc. and Surveying, Ohio State Univ., Columbus
- Pavlis NK, Holmes SA, Kenyon SC, Factor JK (2008) An Earth Gravitational Model to Degree 2160: EGM2008. EGU General Assembly, Vienna, Austria, 13–18 April 2008
- Ramillien G (2002) Gravity/magnetic potential of uneven shell topography. *J Geod* 76(3):139–149
- Rapp RH, Pavlis NK (1990) The development and analysis of geopotential coefficient Models to spherical harmonic degree 360. *J Geophys Res* 95(B13):21885–21911
- Rummel R, Rapp RH, Stükel H, Tscherning CC (1988) Comparisons of global topographic-isostatic models to the Earth's observed gravity Field. Rep. N0. 388, Dpt. of Geodetic Sc. and Surveying, Ohio State Univ., Columbus
- Torge W (2001) *Geodesy*, 3rd edn. de Gruyter, The Netherlands
- Tsoulis D (2001) Terrain correction computations for a densely sampled DTM in the Bavarian Alps. *J geod* 75(5/6):291–307
- Wenzel G (1998) Ultra-high degree geopotential models GPM98A, B and C to degree 1800. Joint meeting of the Intern. Gravity Commission and Intern. Geoid Commission, 7–12 September, Trieste
- Wieczorek MA (2007) Gravity and topography of the terrestrial planets. In: *Treatise on geophysics*, vol 10. Elsevier, Amsterdam, pp 165–206
- Wieczorek MA, Phillips RJ (1998) Potential anomalies on a sphere: applications to the thickness of the lunar crust. *J Geophys Res* 103(E1):1715–1724
- Wigner EP (1959) Group theory and its application to quantum mechanics of atomic spectra. Academic Press, New-York